Electron-Nuclear Double Resonance (ENDOR)
&
Dynamic Nuclear Polarization (DNP)

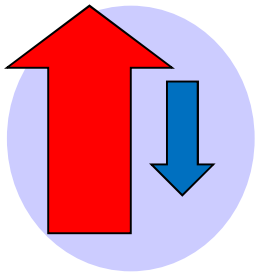

Marina Bennati

MPI Biophysical Chemistry & Göttinger University

EF-EPR School, Brno 2019

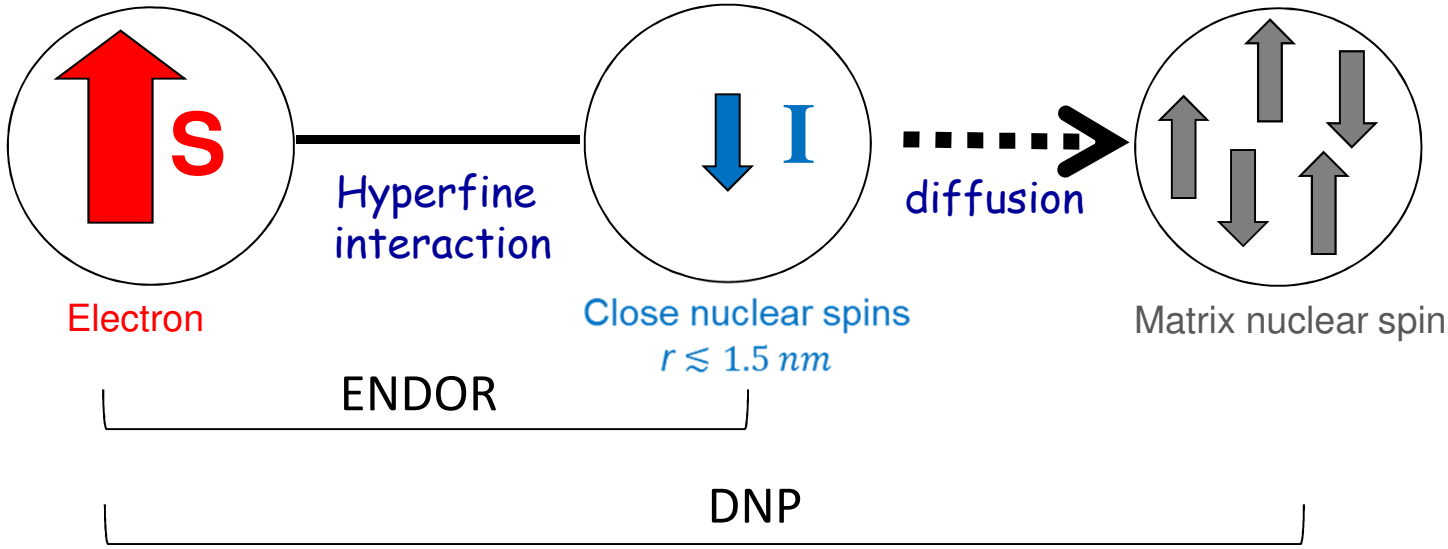

Part I: ENDOR Spectroscopy

- Introduction
- Line shapes of ENDOR spectra
- Examples for applications
- Orientation selection
- Pulse sequences
    - Davies ENDOR (Appendix: theoretical description)
        - effect of the preparation pulse
        - spectral hole and matrix peak
        - Rabi oscillation, RF pulse lengths and resolution
    - Mims ENDOR (Appendix: theoretical description)
    - Triple ENDOR
- Relaxation effects in ENDOR
- New pulse sequences: cross-polarization

Part II: Overview of DNP

- Introduction
- Overhauser DNP in liquid NMR
- MAS DNP in solid-state NMR
- Dissolution DNP in MRI

Part I: Introduction to ENDOR

Electron-nuclear double resonance

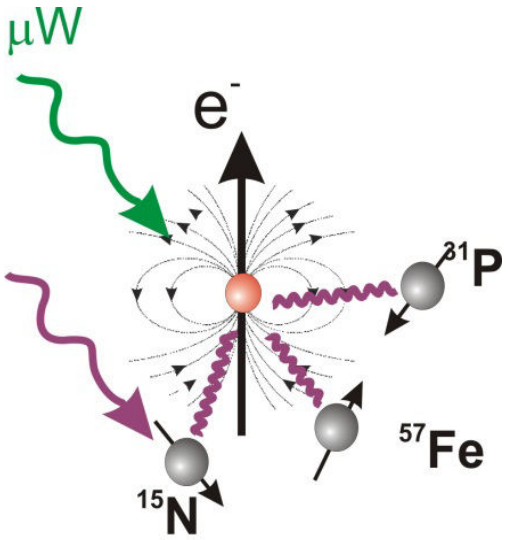

At high fields/high EPR frequencies: increased resolution, ‚first order' spectra, simpler analysis

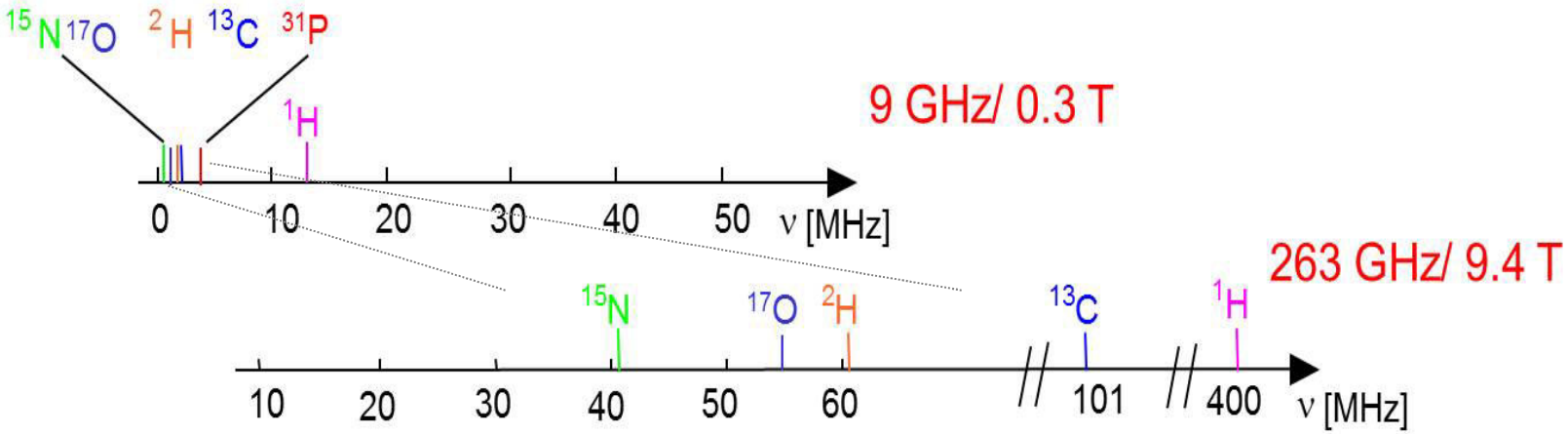

Reminder: Hyperfine Coupling, Basic Definitions

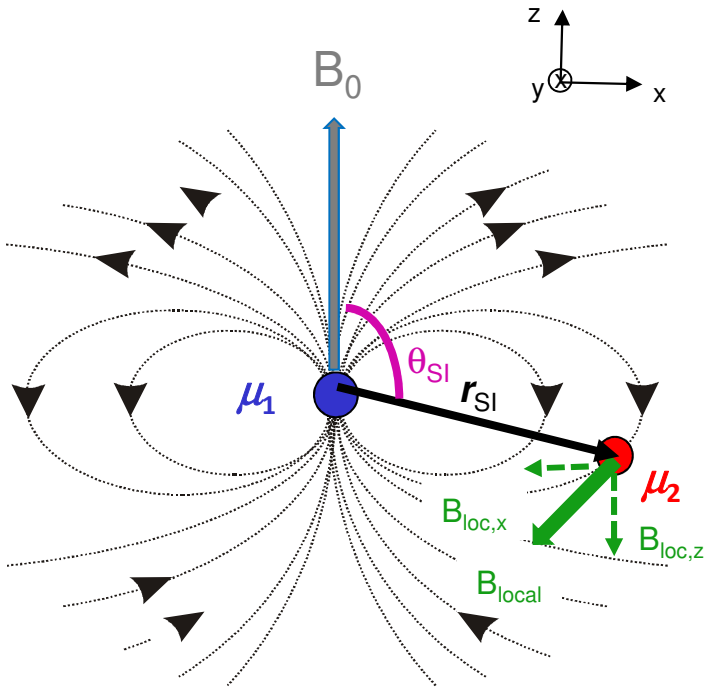

$$\hat{H}_{\mathrm{hf}} = \hat{\boldsymbol{S}} \cdot \boldsymbol{A} \cdot \hat{\boldsymbol{I}} \qquad \boldsymbol{A}_{\mathrm{Diag}} = a_{iso} + \boldsymbol{T} = a_{iso} + \begin{pmatrix} T_{\perp} & & \\ & T_{\perp} & \\ & & T_{\parallel} \end{pmatrix}$$

$T_{||} = -2T_{\perp}$

$\boldsymbol{T}$ is dipolar tensor

Spin Hamiltonian and ENDOR Transitions

General spin Hamiltonian for *k* coupled nuclear spins

$$\hat{H} = \mu_B \boldsymbol{B}\cdot\boldsymbol{g}\cdot\hat{\boldsymbol{S}} + \sum_k \left(-\mu_N g_n^k \boldsymbol{B}\cdot\hat{\boldsymbol{I}} + \hat{\boldsymbol{S}}\cdot\boldsymbol{A}^k\cdot\hat{\boldsymbol{I}} \right)$$

Electron Zeeman **Nuclear Zeeman** **Hyperfine Interaction**

Consider only two ½ spins, approximation for electron: neglect S_x and S_y

$$\hat{H} \approx \mu_B g_e B_0 \hat{S}_z - \mu_N g_n B_0 \hat{I}_z + A_{zz}\hat{S}_z\hat{I}_z + A_{zy}\hat{S}_z\hat{I}_y + A_{zx}\hat{S}_z\hat{I}_x \qquad A_{Lab} = R(\varphi,\theta,0)\cdot A_{Diag}\cdot R^{-1}(\varphi,\theta,0)$$

$$m_S = {}^1/_2\,(\alpha_e) \text{ or } {}^{-1}/_2\,(\beta_e)\,; m_I = {}^1/_2\,(\alpha_n) \text{ or } {}^{-1}/_2\,(\beta_n)$$

Hamiltonian in matrix form
Note the order of elements, is not arbitrary

$$\begin{array}{c|cccc} & |\alpha_e\alpha_n\rangle & |\alpha_e\beta_n\rangle & |\beta_e\alpha_n\rangle & |\beta_e\beta_n\rangle \\ \langle\alpha_e\alpha_n| & \frac{1}{2}\mu_B g_e B_0 - \frac{1}{2}\mu_N g_n B_0 + \frac{A_{zz}}{4} & \frac{1}{4}(A_{zx} - iA_{zy}) & 0 & 0 \\ \langle\alpha_e\beta_n| & \frac{1}{4}(A_{zx} + iA_{zy}) & \frac{1}{2}\mu_B g_e B_0 + \frac{1}{2}\mu_N g_n B_0 - \frac{A_{zz}}{4} & 0 & 0 \\ \langle\beta_e\alpha_n| & 0 & 0 & -\frac{1}{2}\mu_B g_e B_0 - \frac{1}{2}\mu_N g_n B_0 - \frac{A_{zz}}{4} & -\frac{1}{4}(A_{zx} - iA_{zy}) \\ \langle\beta_e\beta_n| & 0 & 0 & -\frac{1}{4}(A_{zx} + iA_{zy}) & -\frac{1}{2}\mu_B g_e B_0 + \frac{1}{2}\mu_N g_n B_0 + \frac{A_{zz}}{4} \end{array}$$

S =1/2, *I* = ½

High field approximation (first order): neglect also I_x und I_y, i.e. A_{zy} and A_{zx}

$$\Delta E_{\text{EPR,allowed}} \approx \mu_B g_e B_0 \pm \frac{1}{2}A_{zz} \qquad (\Delta m_S = 1)$$

$$\Delta E_{\text{ENDOR}} \approx \mu_N g_n B_0 \pm \frac{1}{2}A_{zz} \qquad (\Delta m_I = 1)$$

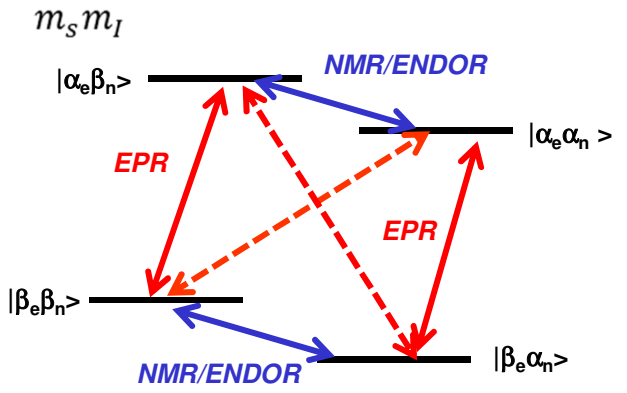

here $g_n > 0$, $A > 0$

S =1/2, I = ½,

Energy $A > 0$, $A < \nu_n$ (weak coupling) $g_n > 0$

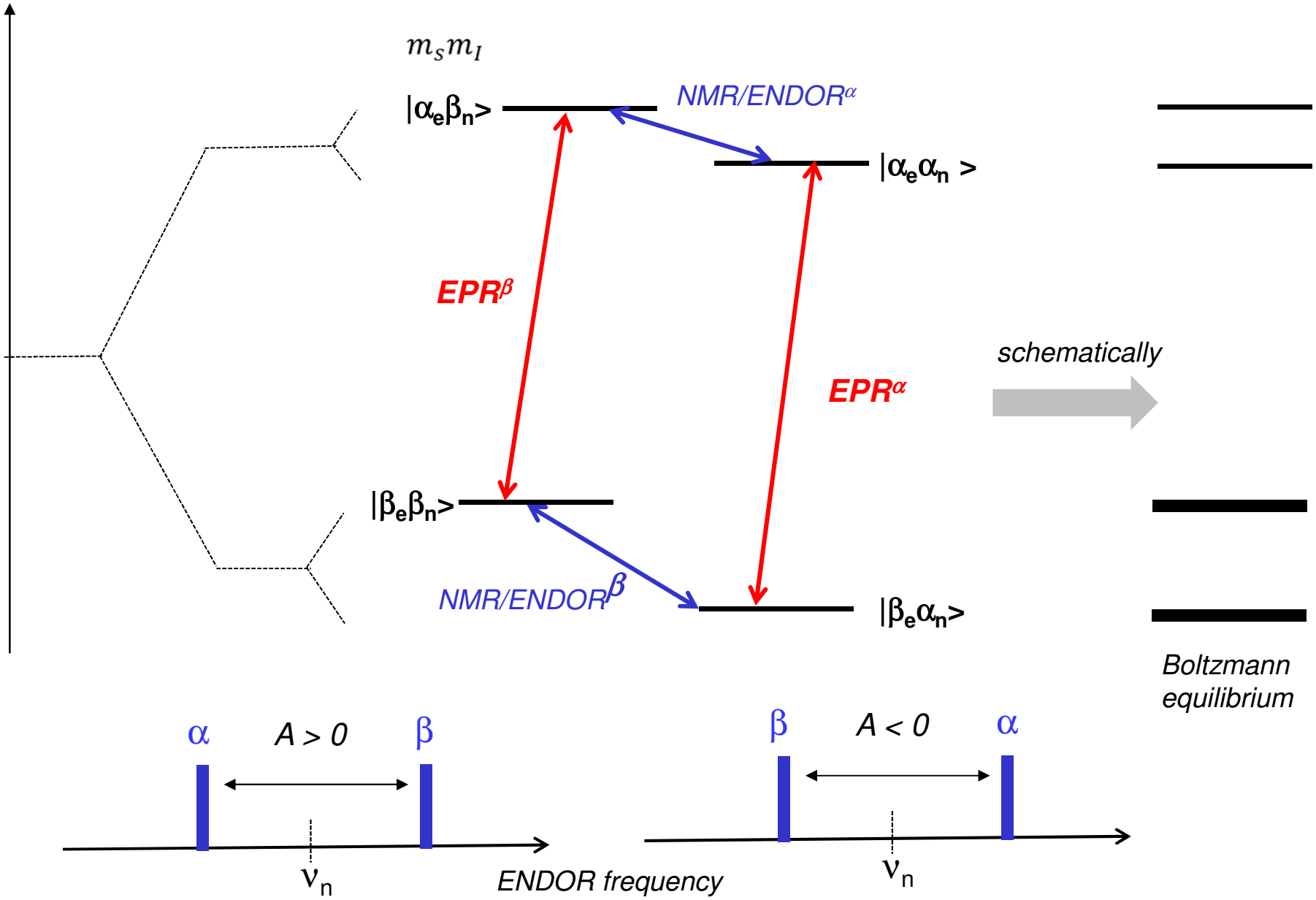

Line Shape of ENDOR Spectra in Powders

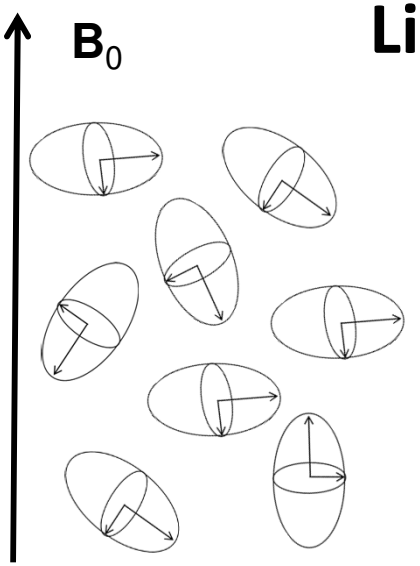

All molecular orientations contributes with same probability

$$\Delta E_{\mathrm{ENDOR}} \approx \mu_{\mathrm{N}} g_{\mathrm{n}} B_0 \pm \frac{1}{2} A_{zz}$$

$$A_{zz} = a_{iso} + (3cos^2\theta - 1) \cdot T_{\perp}$$

$T_{||} = -2T_{\perp}$

T is dipolar tensor

Pake pattern

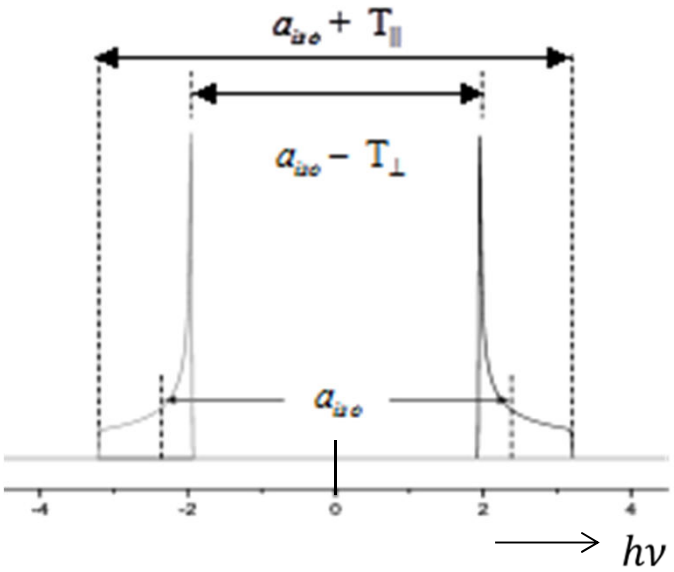

$a_{iso} >> T_{||}$,

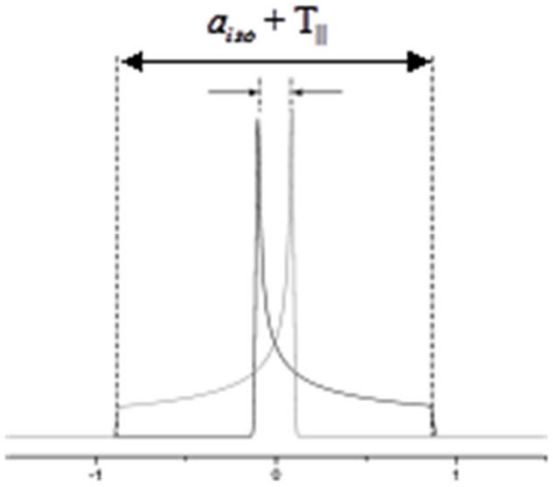

$a_{iso} << T_{||}$

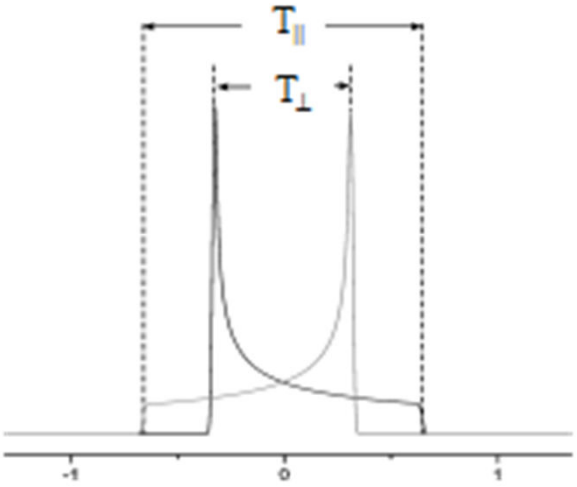

$a_{iso} = 0$

^{31}P ENDOR Spectra of GDP bound to Mn^{2+} in Ras Protein

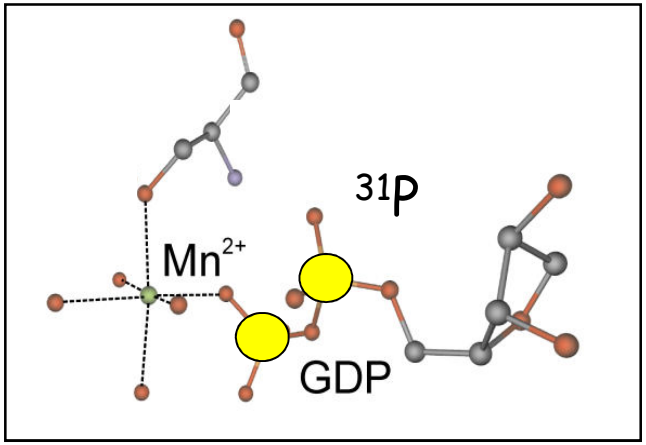

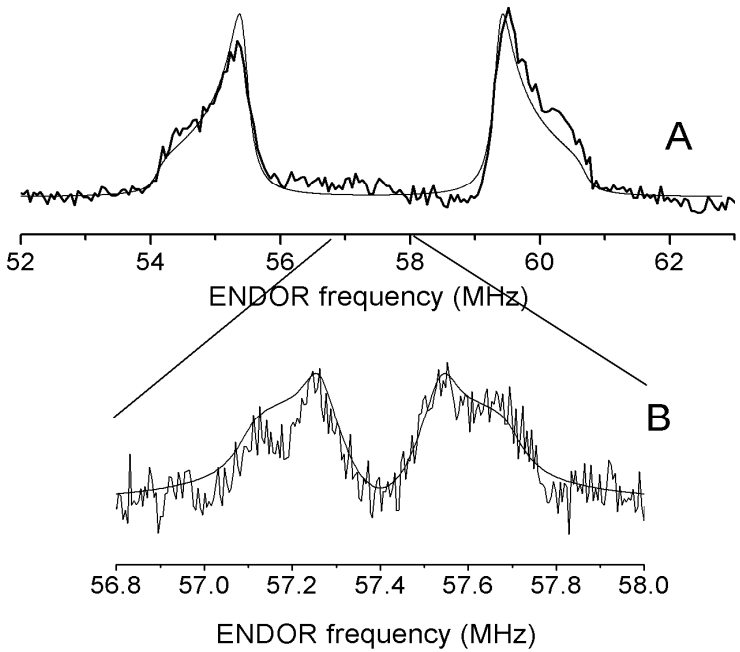

^{31}P I = ½, 100 % abundance
Mg^{2+} → Mn^{2+}
Mn^{2+} ENDOR at W-band (94 GHz)
Two ^{31}P nuclei are visible in ENDOR

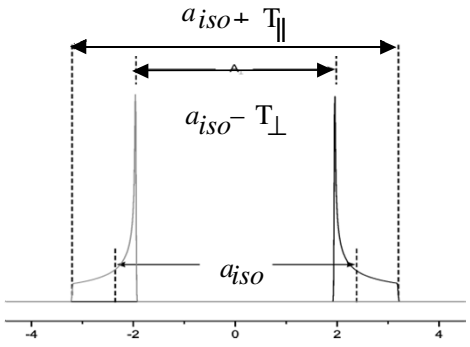

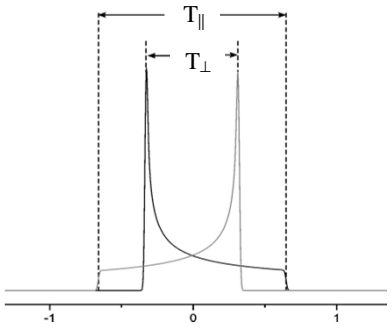

Bennati M. , M. Hertel, Fritscher, Prisner et al. Biochemistry 2006

Example: Distance Measurements with ^{19}F ENDOR

^{19}F I = ½, 100 %

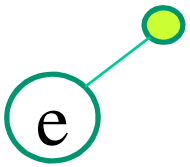

r ≈ 0.5 -1.5 nm

= **^{19}F**

- g_n (^{19}F) ≈ g_n (^{1}H)

  $\Delta\nu_L$ ≈ 8 MHz at 94 GHz

- scarcity in biology

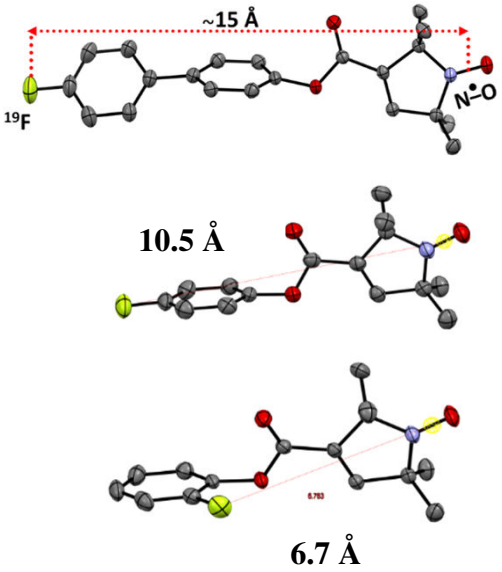

W-band ENDOR
Only dipolar coupling

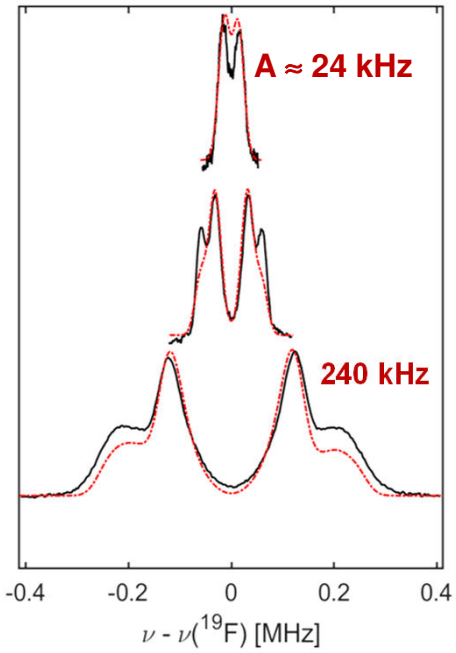

Meyer et al, Angewandte Chemie 2019, doi:10.1002/anie.201908584

Orientation Selection

Only part of EPR spectrum is excited → Incomplete powder ENDOR spectrum

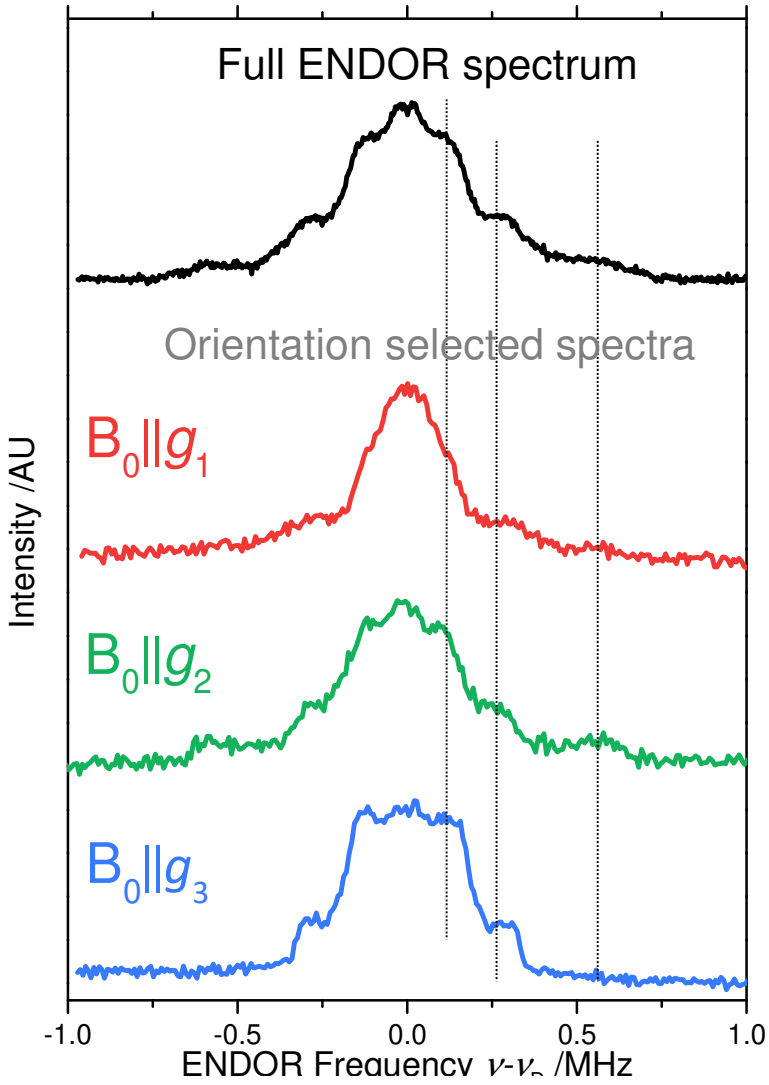

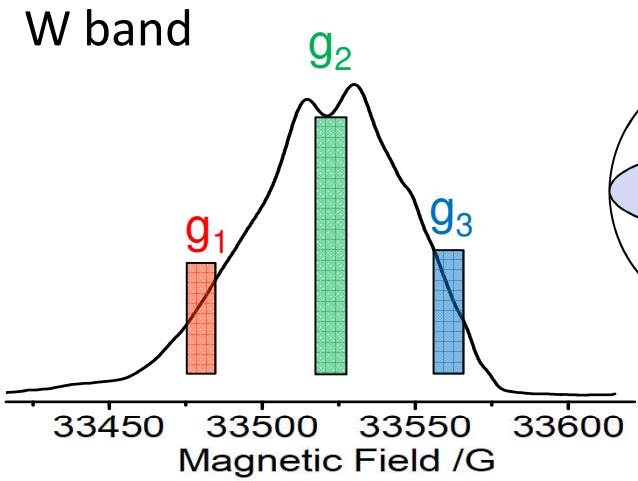

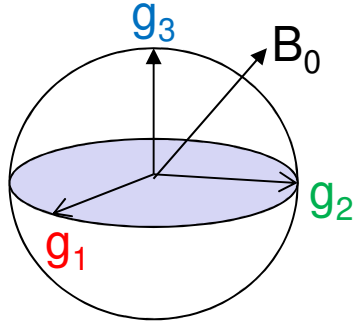

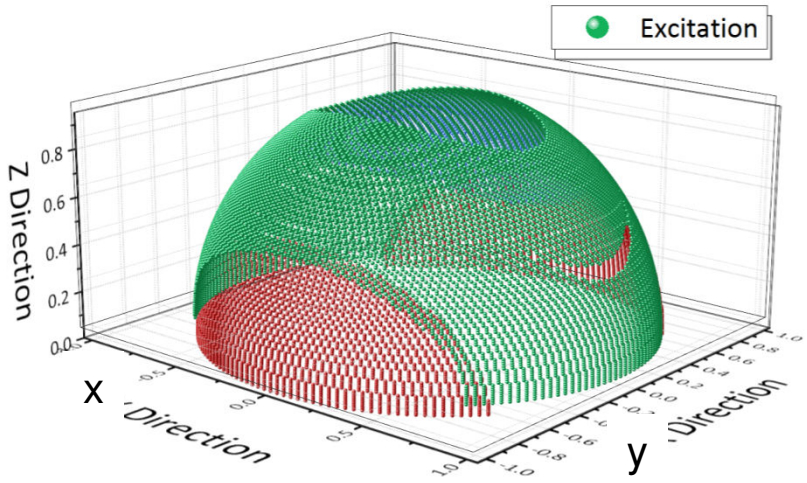

Example for Orientation Selection

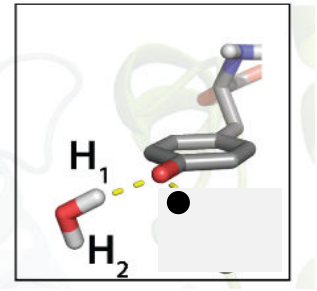

Example:
Tyrosyl radical, hydrogen bond
$H_2O \rightarrow D_2O$ exchange
140 GHz ^2H ENDOR

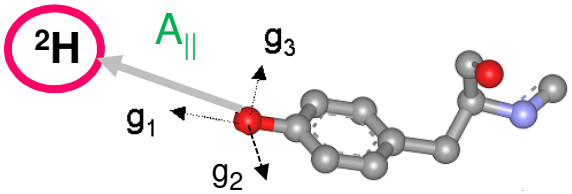

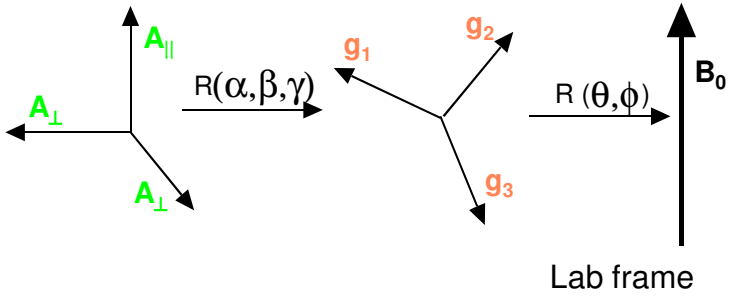

Bar et al. JACS 2001

Enhanced Resolution via Orientation Selection

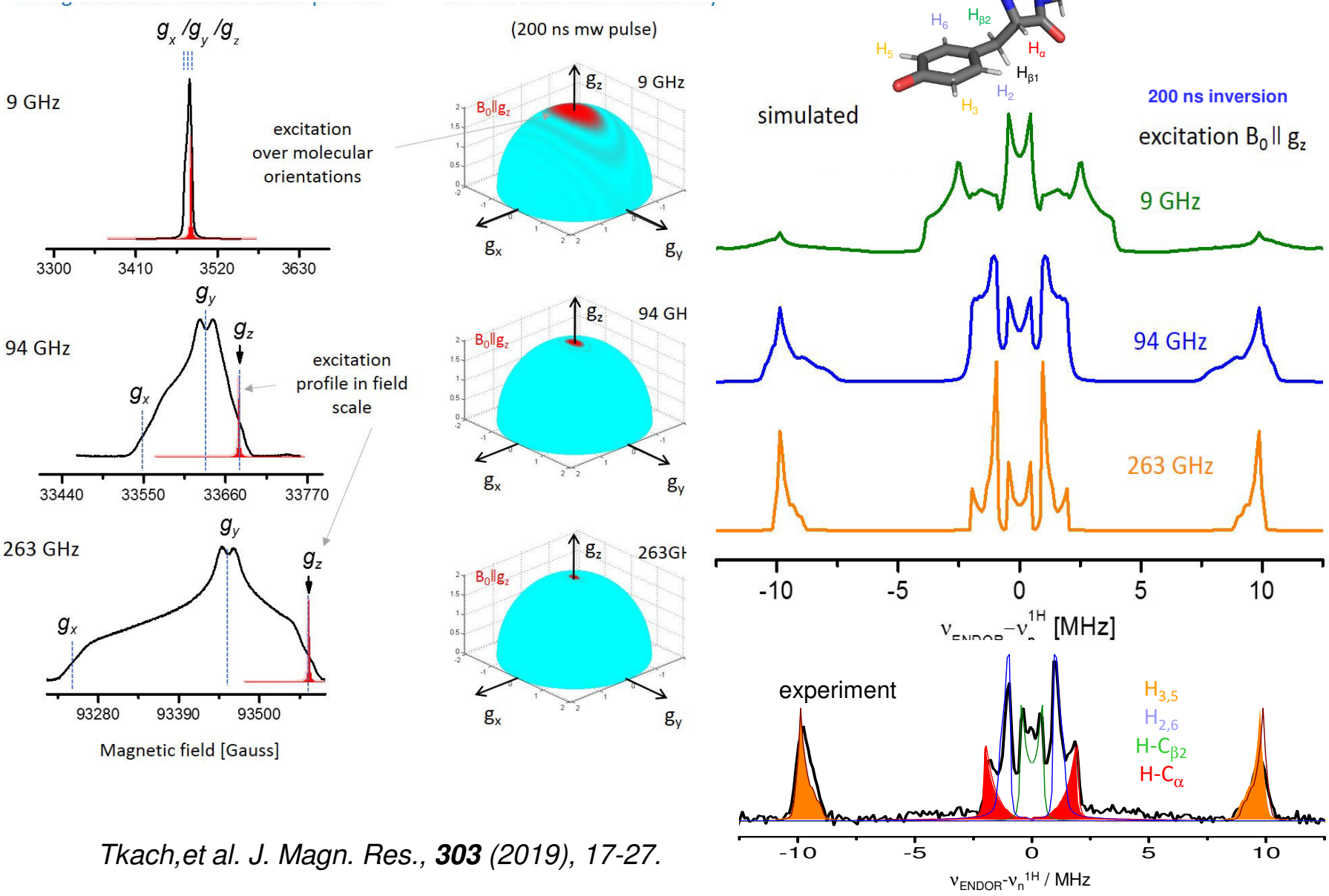

Tkach,et al. J. Magn. Res., ***303*** *(2019), 17-27.*

Choice of Frequency

Comparison Q band and W band

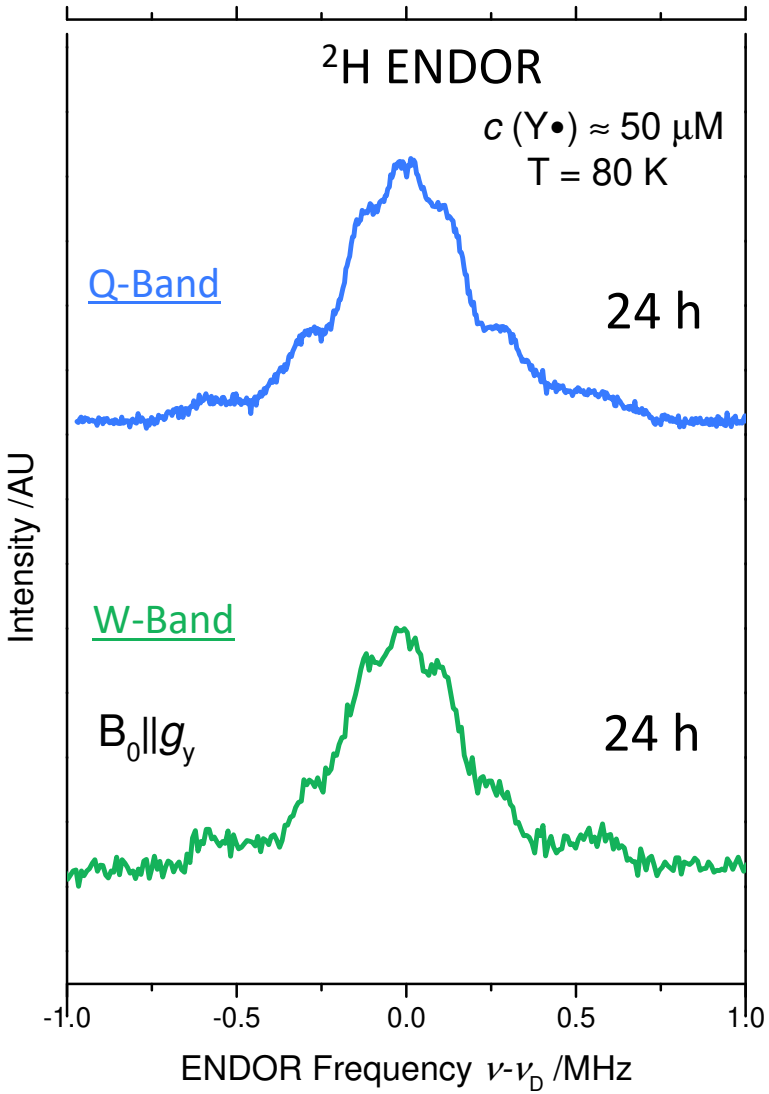

Excite (almost) full EPR spectrum (organic radicals)

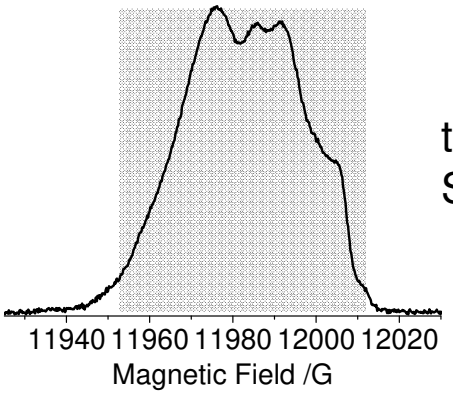

$t_{\pi/2}$ = 6 – 10 ns
Sample volume: 10 µL

Orientation selection

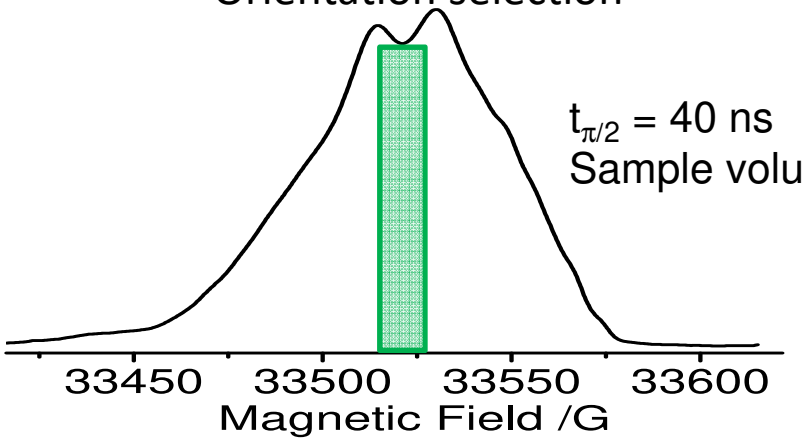

$t_{\pi/2}$ = 40 ns
Sample volume: 2 µL

S/N decreases in W-band only by a factor of 3

Pulse Techniques to Record ENDOR Spectra

Also CW ENDOR (see References)

General principles and scheme:
population/polarization transfer between allowed EPR and NMR transitions

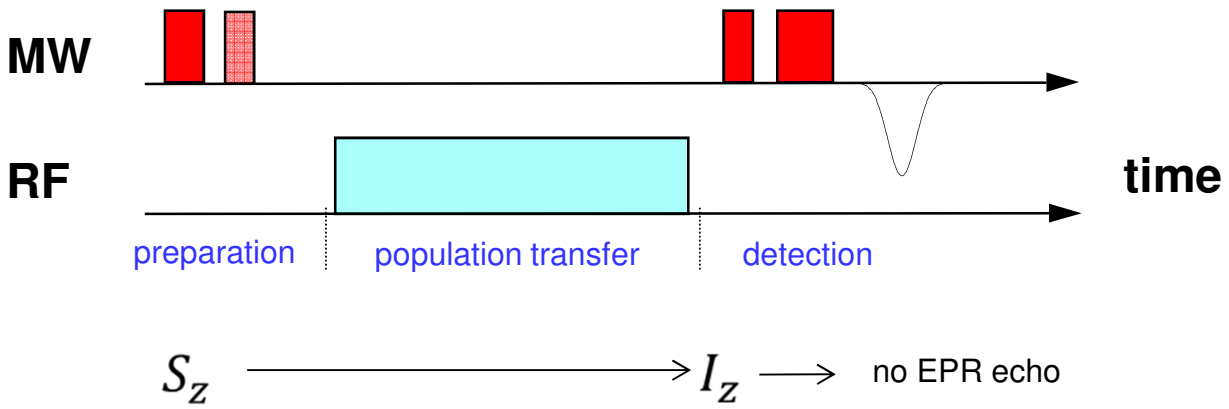

- Usually, no need of very strong MW pulses
- Resolution is limited by RF pulse, T_{1e}, electronic T_M, spectral diffusion
- Sensitivity is limited by T_{1e}, T_{1n} (repetition time), hf anisotropy

Davies ENDOR

Davies, Phys. Rev. Lett. A, 47,1-2 (1974)

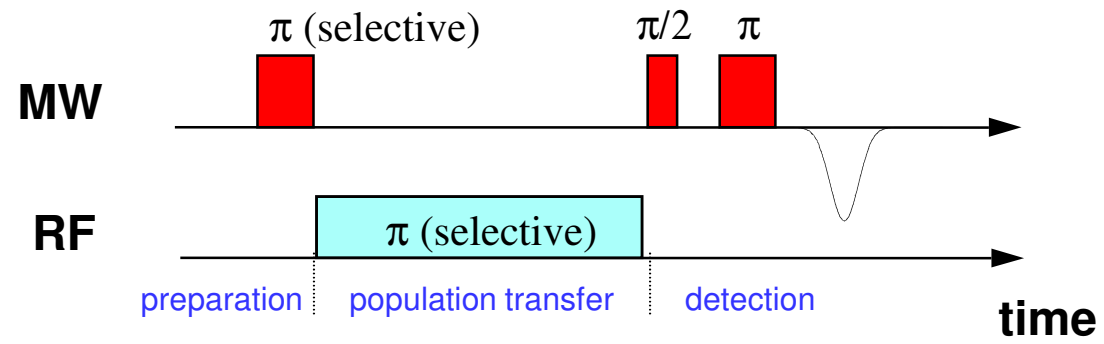

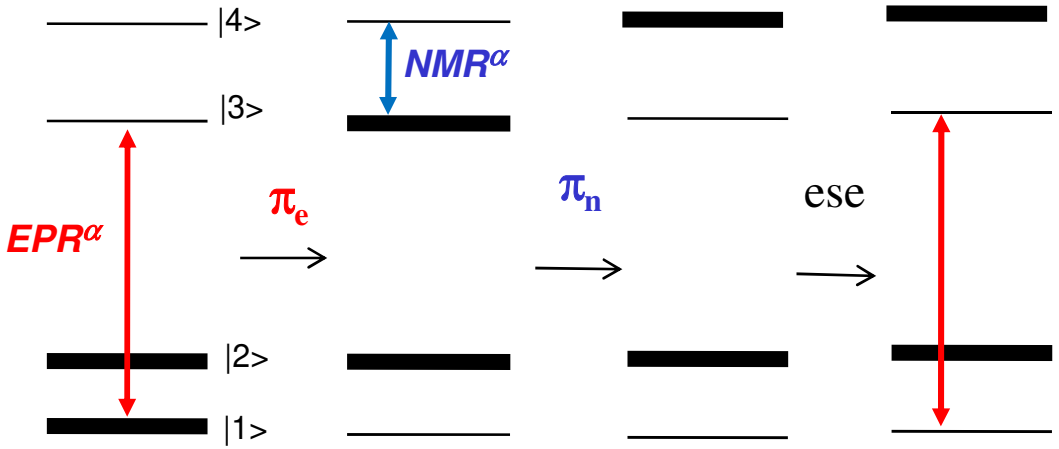

- Selective π-pulses invert populations of EPR and NMR/ENDOR transitions.
- EPR echo intensity is recorded as a function of the NMR/ENDOR frequency.
- Very good performance for: large couplings $A \gtrsim$ 3-4 MHz, Orientation selection

Appendix: Description with Product Operators

C. Gemperle & A. Schweiger, Chem. Rev. 1991, Vol. 91, p. 1481

$\mathcal{H} = H/\hbar$ Hamiltonian in frequency units

$\mathcal{H}_0 = \Omega\, S_z + \Delta\omega_n I_z + a I_z S_z$ Doubly rotating frame Hamiltonian

$\mathcal{H}_1^{\alpha} = \omega_1 S_x I^{\alpha}$ Selective MW pulse on α nuclear spin manifold

$\mathcal{H}_1^{\beta} = \omega_2 S^{\alpha} I_x$ Selective RF pulse on α electron spin manifold

$\sigma(t) = \sum_n b_n(t) B_n$ Reduced density operator as a linear combination of product operators

$\dot{\sigma}(t) = -i[\mathcal{H}(t), \sigma(t)]$ Liouville-von Neumann equation for time evolution of σ

$\sigma(t + t_1 + t_2) = e^{-i\mathcal{H}_2 t_2} e^{-i\mathcal{H}_1 t_1} \sigma(t) e^{+i\mathcal{H}_1 t_1} e^{+i\mathcal{H}_2 t_2}$ Solution for time-independent Hamiltonians

$\sigma(0) \xrightarrow{\mathrm{H}^{(1)}\tau_1} \sigma(\tau_1) \xrightarrow{\mathrm{H}^{(1)}\tau_2} \ldots$ ⇒ $B_n \xrightarrow{\varphi B_m} B_n \cos\varphi - i[B_m, B_n]\sin\varphi$

Davies ENDOR preparation:

$$-S_z = -S_z I^{\alpha} - S_z I^{\beta} \xrightarrow{\pi S_x I^{\alpha}} S_z I^{\alpha} - S_z I^{\beta} = 2 S_z I_z = \sigma_{prep}^{sel}$$

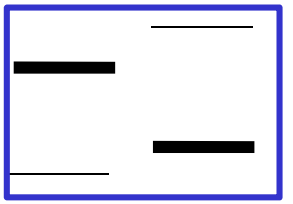

Electron-nuclear two-spin order

Echo intensity as a function of RF pulse with angle β_2:

$$\sigma_{prep}^{sel} \xrightarrow{\beta_2 S^{\alpha} I_x} \xrightarrow{(\pi/2) S_x I^{\alpha}} \xrightarrow{\mathrm{H}_0 \tau} \xrightarrow{\pi S_x I^{\alpha}} S_y I^{\alpha} \left[\frac{1}{2}(1 + \cos\beta_2)\right]$$

Davies ENDOR Efficiency

ENDOR efficiency:

$$F_{ENDOR} = \frac{1}{2}\left|\frac{I_{echo}(rf\_off) - I_{echo}(rf\_on)}{I_{echo}(rf\_off)}\right| \qquad 1 > F_{ENDOR} > 0$$

Maximal Davies ENDOR efficiency: 0.5

Davies ENDOR with optimized efficiency (*F = 1*):

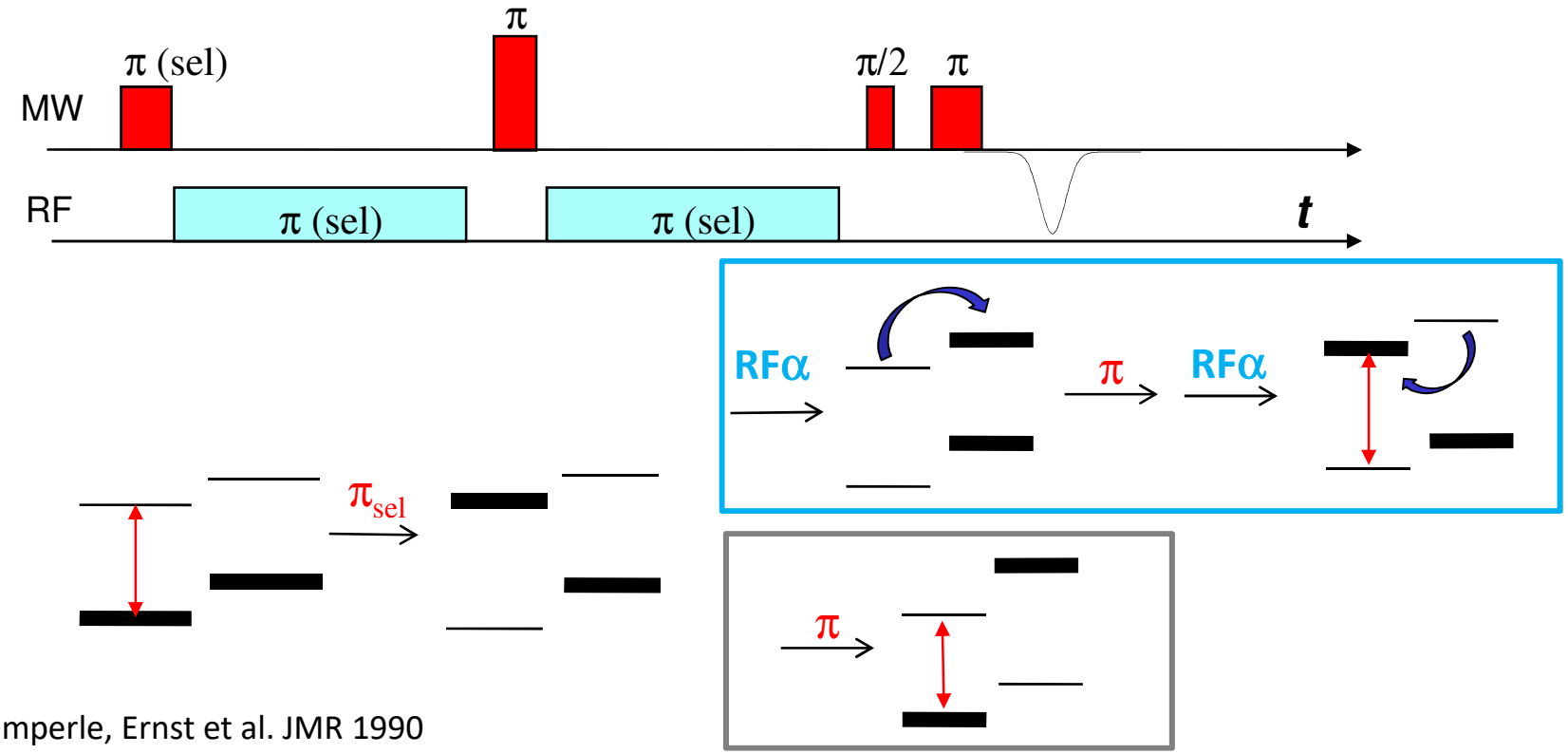

Gemperle, Ernst et al. JMR 1990

Effect of Preparation Pulse in Powders

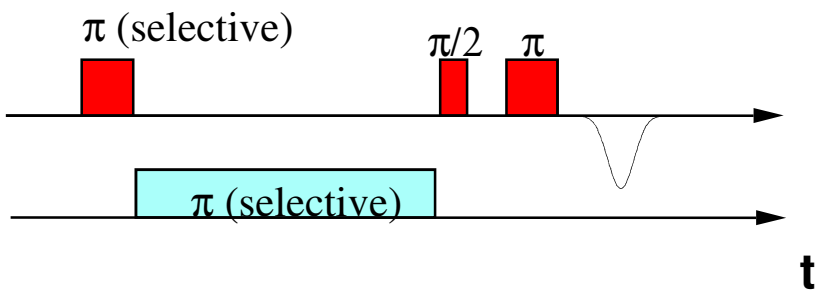

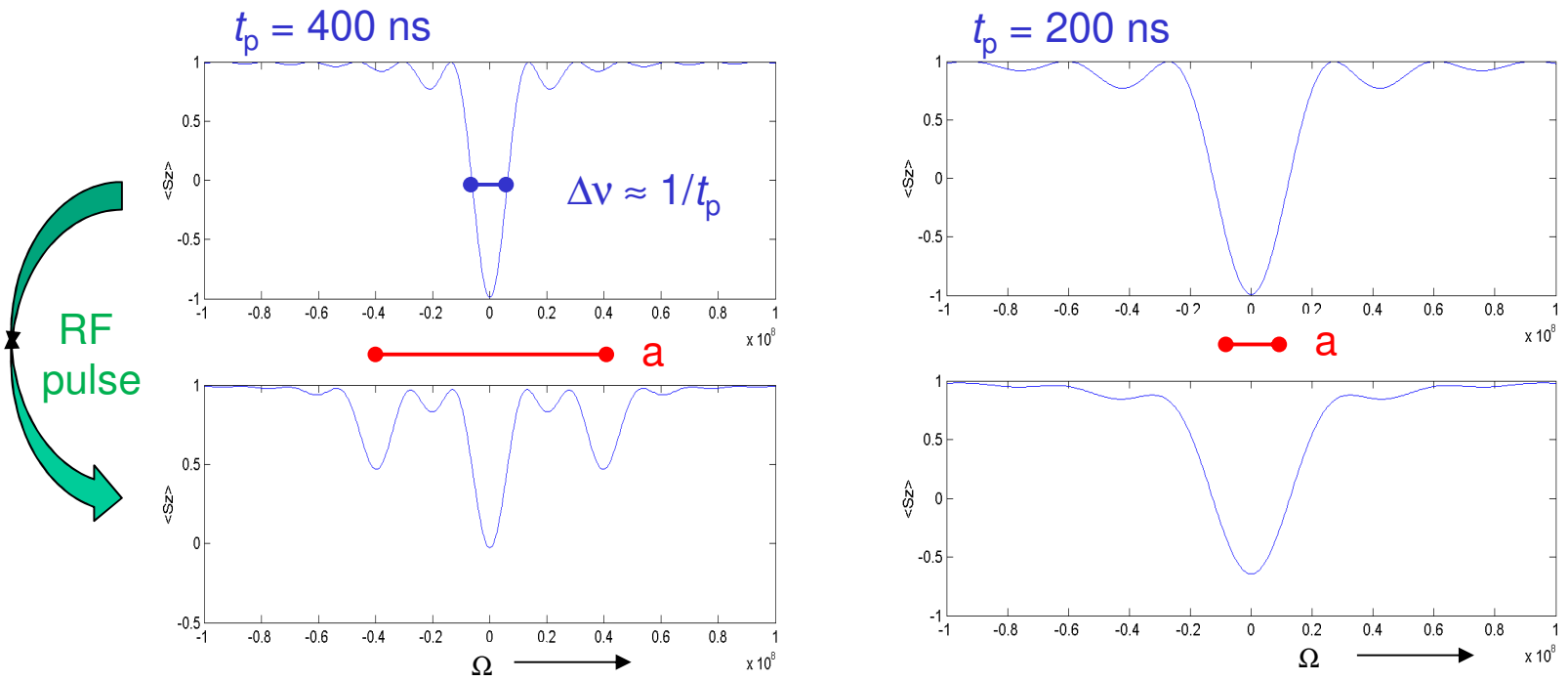

Top: Calculated $\langle S_z \rangle$ after a π-pulse of 400 ns and 200 ns (left and right, respectively).
Bottom: $\langle S_z \rangle$ after a RF π-pulse with frequency A = 6.3 MHz (left) and 1.6 MHz (right).

Simple Explanation: Four Spin Packets

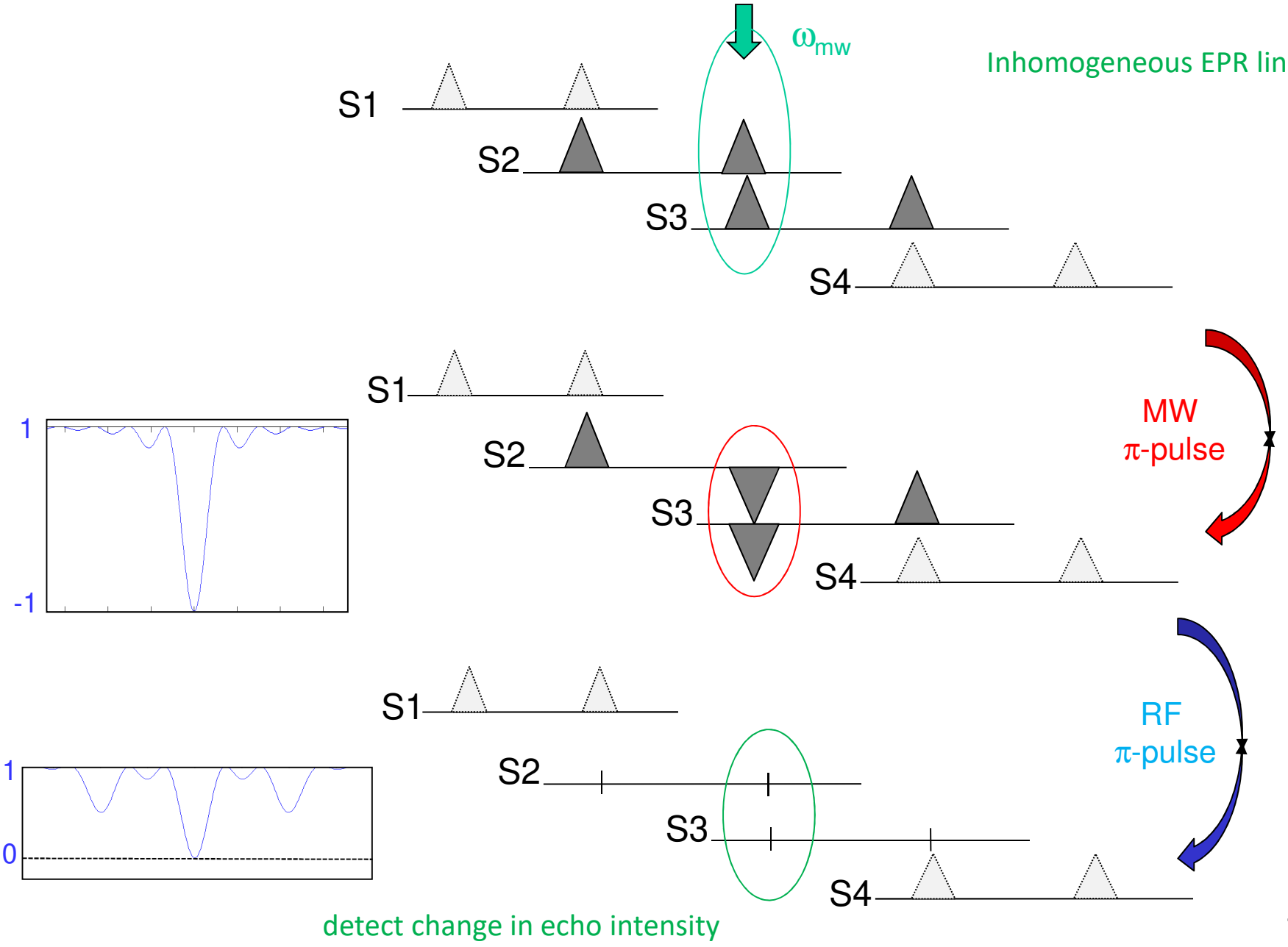

Example: Hyperfine Selective ENDOR

Separate overlapping ENDOR lines

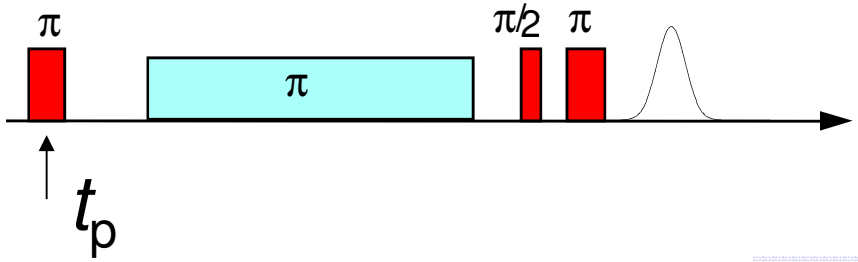

a (^{57}Fe) ≈ 30 – 40 MHz ν_L (^{57}Fe) = 0.5 MHz
Strong coupling regime
a (^{1}H) ≈ 5 – 10 MHz ν_L (^{1}H) = 14.5 MHz

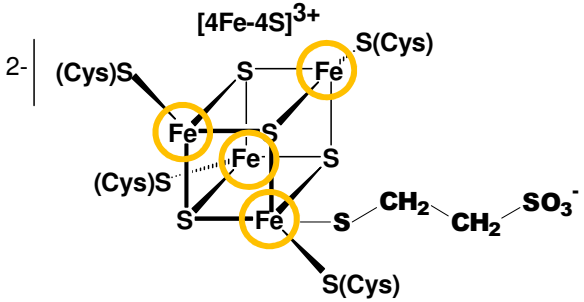

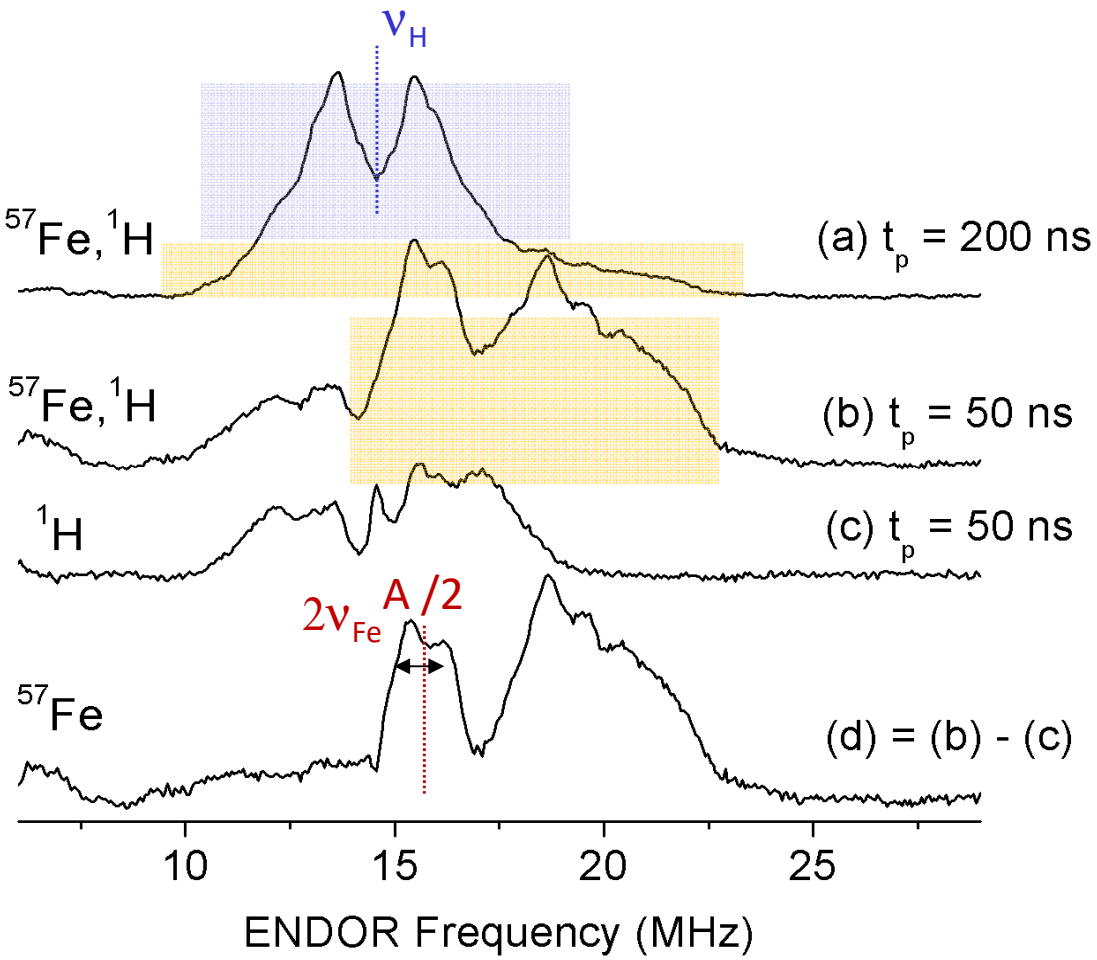

Bennati et al. JACS 2004

Optimizing RF Pulse Length

Pulse length determines resolution (line width $\Delta = 1/t_{p,RF}$) of spectrum

$$\beta_2 = \omega_2 t_p = \gamma_2 B_2 t_p$$

Pulse length/B_2 depends on RF circuit, RF-amplifier and on effective RF penetration in the resonator (if coil is placed outside).

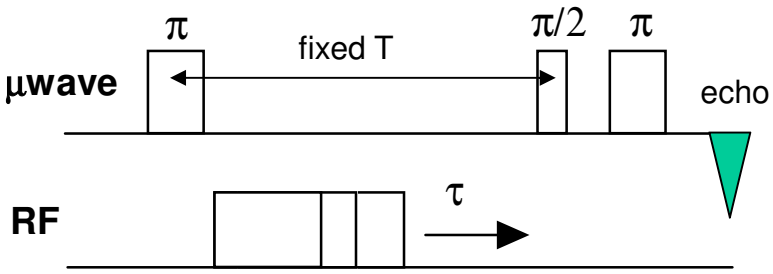

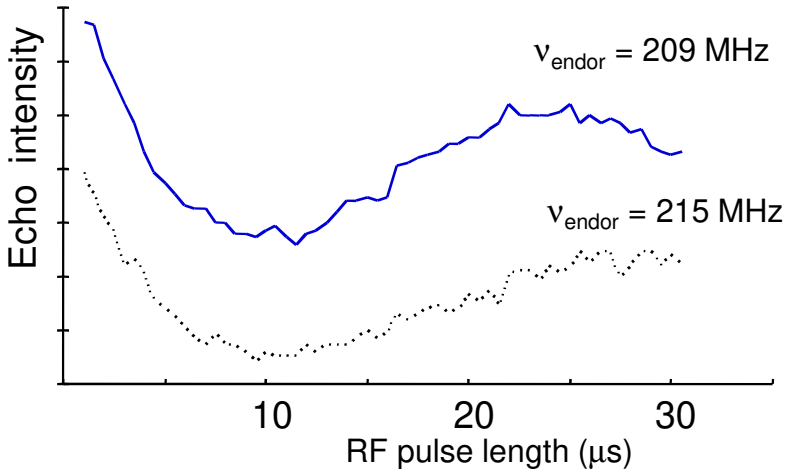

^{1}H Rabi oscillation recorded on two different ENDOR lines of BDPA at 5 Tesla (ν_{proton} = 211 MHz). P_{RF} = 400 W.

Mims ENDOR

Mims, W.B.: Proc. R. Soc. Lond. A 283, 452-457 (1965)

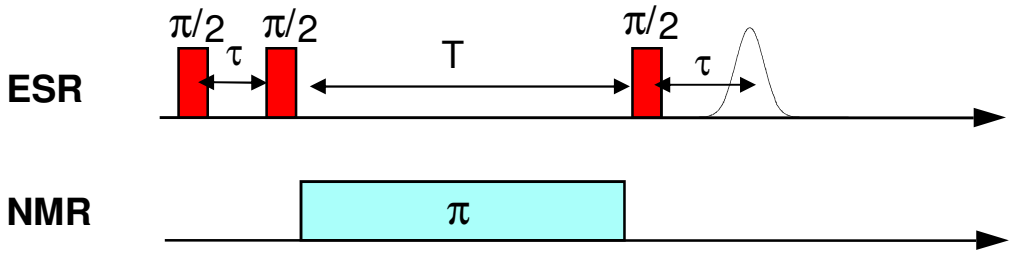

Appendix: Mims ENDOR with Product Operators

)

Echo intensity without RF pulse:

$$\sigma_{prep}^{nonsel} \xrightarrow{H_0\tau} \xrightarrow{(\pi/2)S_x} \xrightarrow{H_0\tau}$$

$$-S_y\{\cos^2[(a/2)\tau]\cos^2[\Omega\cdot\tau]+\sin^2[(a/2)\tau]\sin^2[\Omega\cdot\tau]\}=\sigma_{echo}^{rf\_off}$$

Echo intensity with RF pulse:

$$\sigma_{prep}^{nonsel} \xrightarrow{\beta_2 S^{\alpha} I_x} \xrightarrow{(\pi/2)S_x} \xrightarrow{H_0\tau}$$

$$-S_y\left\{\cos^2[(a/2)\tau]\cos^2[\Omega\cdot\tau]+\sin^2[(a/2)\tau]\sin^2[\Omega\cdot\tau]\frac{1}{2}(1+\cos\beta_2)\right\}=\sigma_{echo}^{rf\_on}$$

for $\beta_2 = \pi$, this term goes to zero:

Echo intensity for $\beta_2 = \pi$:

$$\sigma_{echo}^{rf\_\pi} = -S_y\{\cos^2[(a/2)\tau]\cos^2[\Omega\cdot\tau]\} \xrightarrow{\text{Average over EPR resonance offsets } \Omega} -S_y\left\{\frac{1}{2}\cos^2[(a/2)\tau]\right\}$$

$$= \frac{1}{4}(1+\cos(a\tau))$$

ENDOR efficiency for $\beta_2 = \pi$:

$$F_{Mims} = \frac{1}{2}\sin^2\left(\frac{a}{2}\tau\right)$$

Blind spots for $\tau = 2n\pi/a$, n = 1,2,..

Examples of Spectra with BDPA

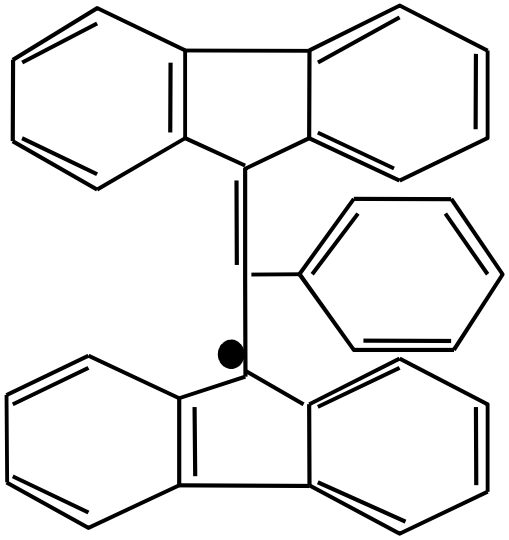

BDPA

(Bis-Diphenylene-Phenyl-Allyl)

BDPA is a stable organic radical with an alternating spin density localized on the diphenylene rings. Two hyperfine couplings result from two sets of eight magnetically equivalent ring protons, yielding a pair of doublets in the ENDOR spectrum. The EPR line at 5 Tesla is nearly Gaussian with a width of about 10 Gauss (almost isotropic g)

$$A_1 = \begin{bmatrix} 7.7 & & \\ & 5.3 & \\ & & 2.0 \end{bmatrix} MHz \quad A_2 = \begin{bmatrix} 1.0 & & \\ & 1.0 & \\ & & 1.26 \end{bmatrix} MHz$$

Comparison of ^{1}H Davies and Mims Spectra

ν (^{1}H) = 211 MHz
B_0 = 5 T
RF pulse = 10 µs
Room temperature

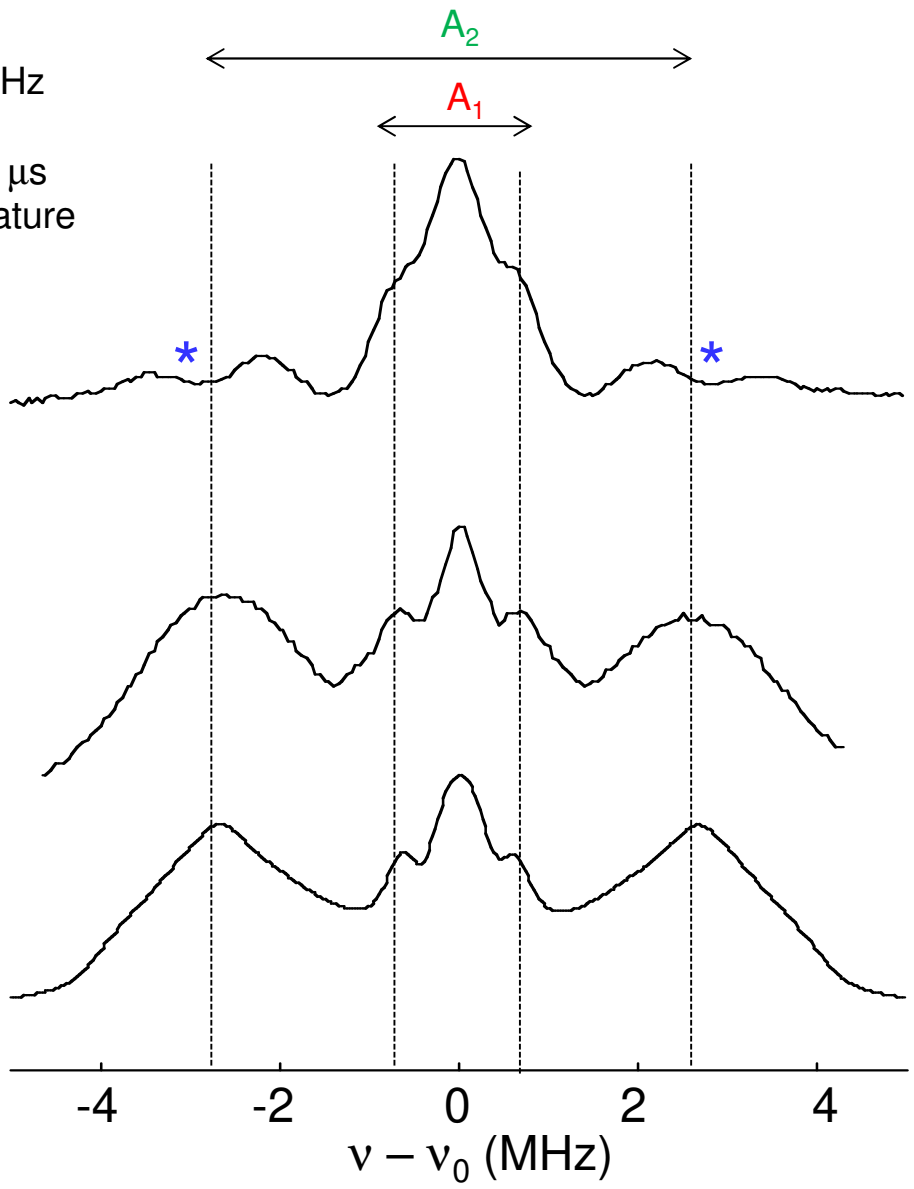

Mims ENDOR
tau = 200ns
$t_{\pi/2}$ = 100 ns

* blind spots

Davies ENDOR
t_π = 200 ns

Davies ENDOR simulation

Pulse TRIPLE Spectroscopy

Measures relative sign of hf coupling

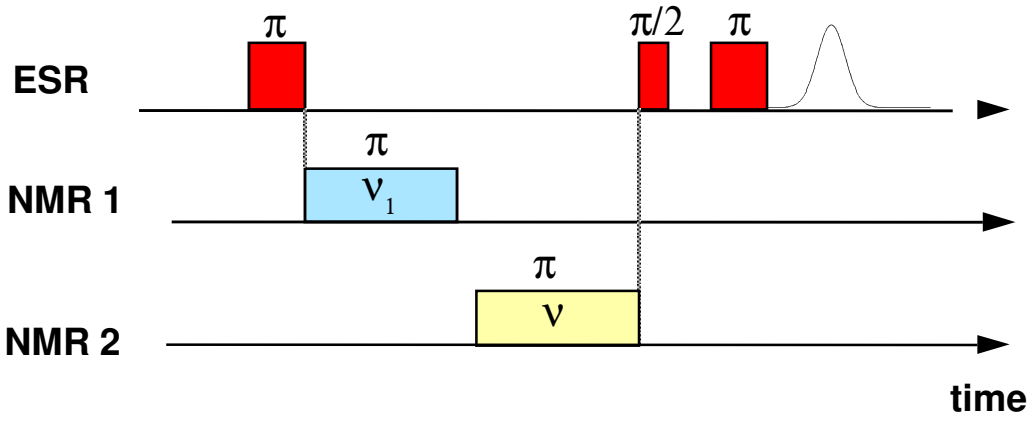

TRIPLE spectroscopy allows for correlation of nuclear sublevels and detection of the relative sign of the hyperfine coupling.

Energy Levels for a S = ½, I_1= ½ I_2 = ½ System

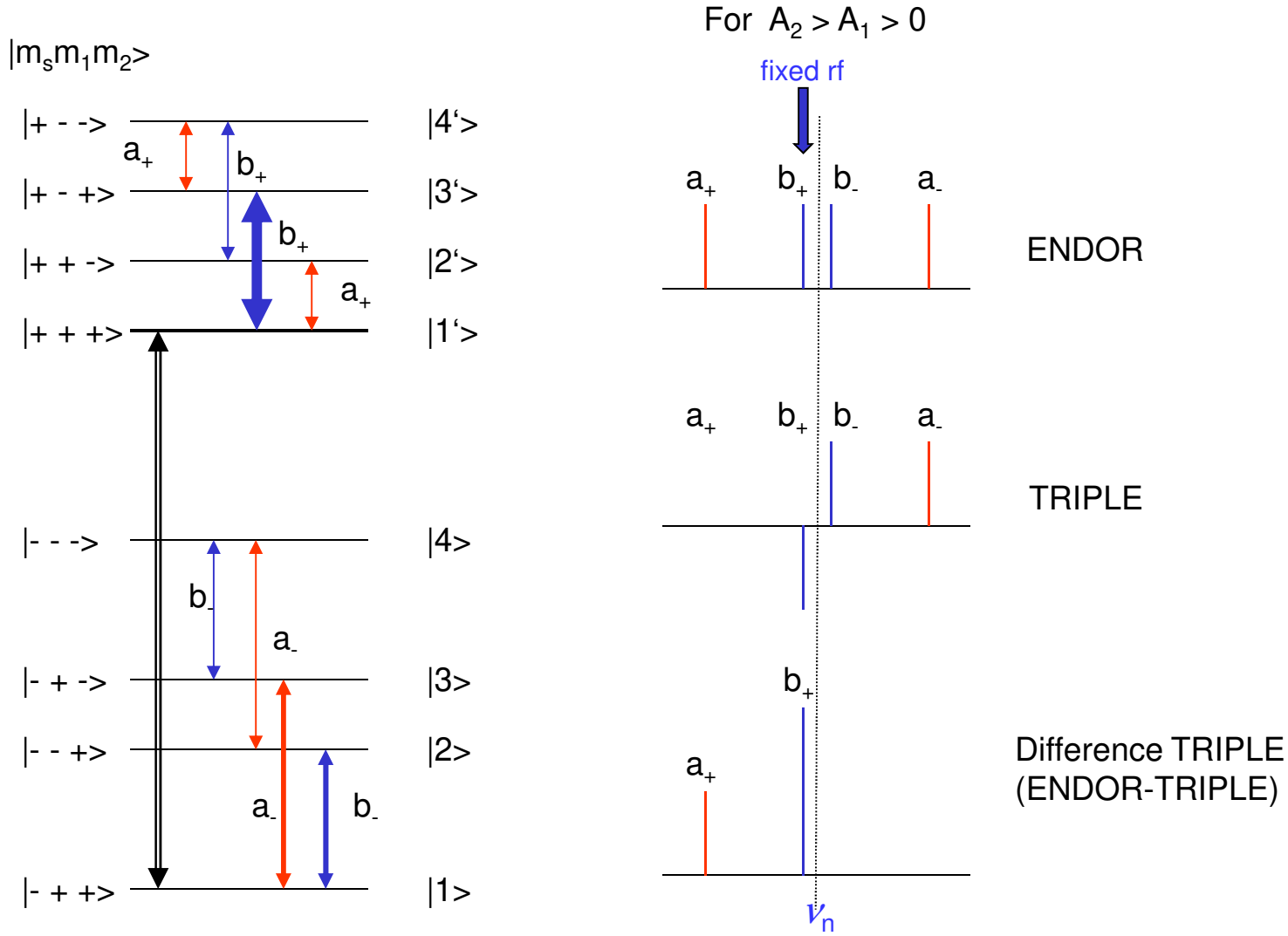

For two hyperfine couplings of same sign, *Difference Triple* gives two ENDOR lines on the same side with respect to the Larmor frequency

Example: Pulse TRIPLE on ^{1}H BDPA

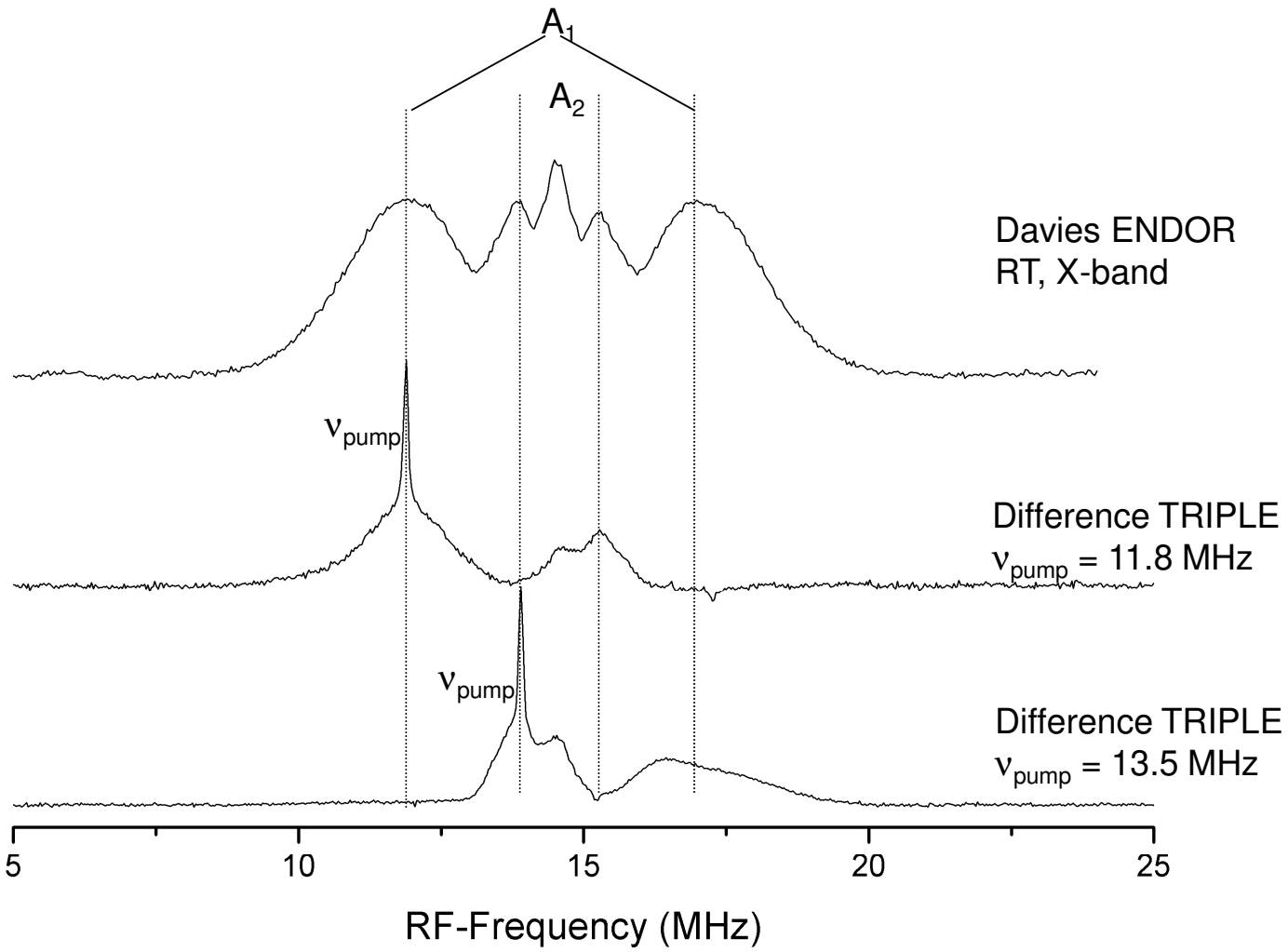

In BDPA the two hyperfine couplings have **opposite** signs

Relaxation Effects in ENDOR

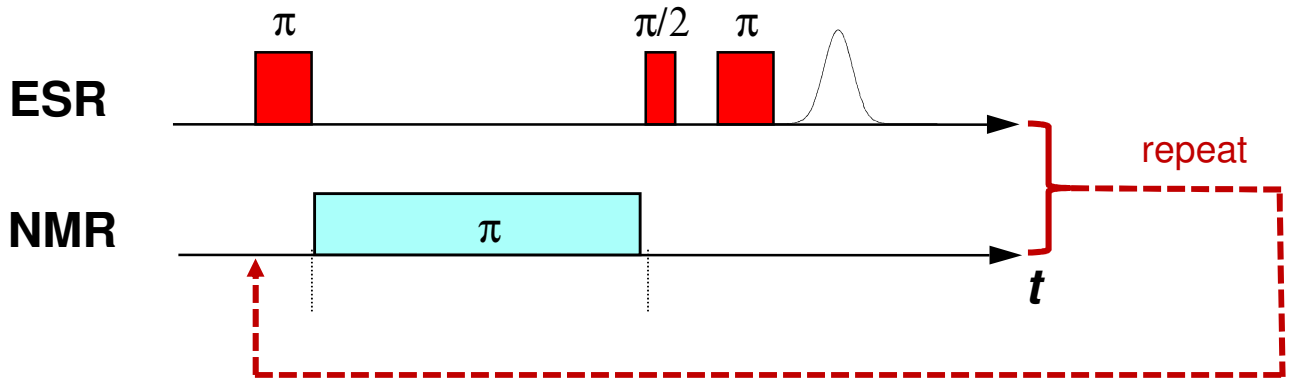

S = 1/2

I = *1/2*

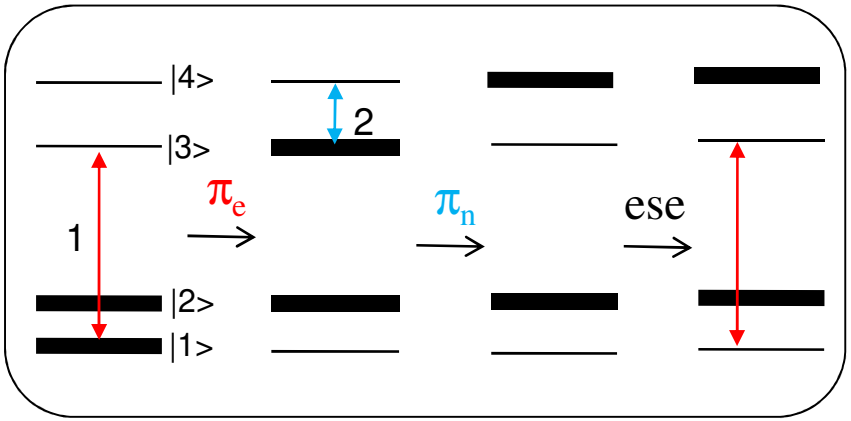

1st shot

F_{endor} = 50%

At very low T:

t_r

$t_r \approx T_{1e}$

$t_r << T_{1n}, T_{1x}$

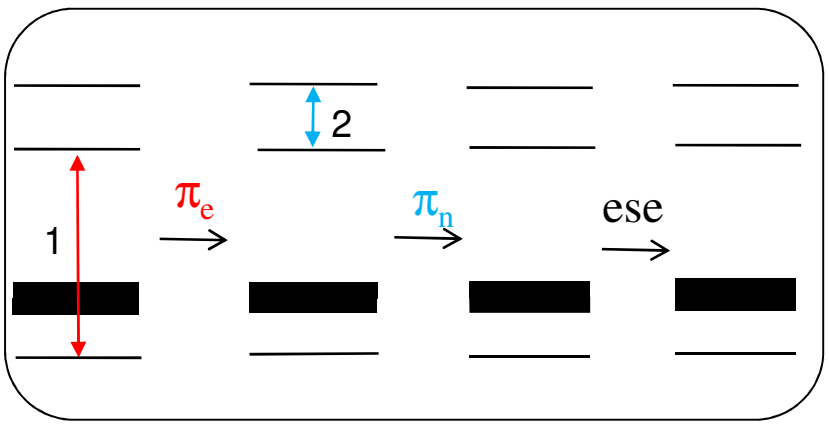

2nd and subsequent shots

$F_{endor} \approx 0\%$

Methods to Overcome Saturation

Random RF acquisition: use **random** rf acquisition and **1 shot/point** if feasible by your hardware. Option is standard in Bruker spectrometers. This might be sufficient to overcome saturation when detecting ^{1}H *(T > 10 K). Experimental* T_{1n} *values not easily accessible.*

TIDY ENDOR: one additional RF pulse is added at end of the Davies or Mims sequence (Tyryshkin, Morton, Lyon et al JCP 2006). Best performance with narrow lines, but less efficient in powders.

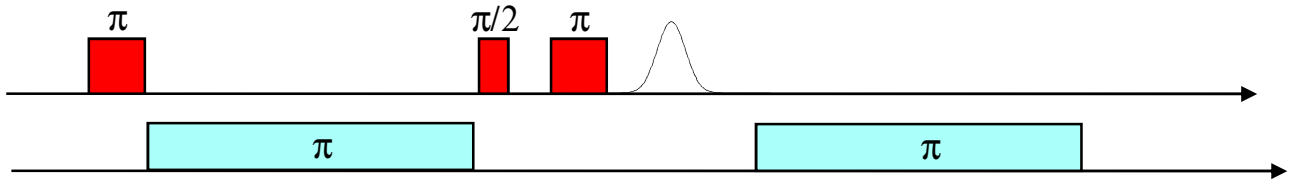

CP-ENDOR: sequence based on cross-polarization produces a non-equal polarization of ENDOR lines and attenuates saturation.
(Rizzato, Kaminker, Vega, Bennati Molecular Physics 2013, Rizzato & Bennati PCCP 2014)

Appendix: Relaxation in ENDOR

- ENDOR deals with populations, only T_{1e}, T_{1n} and T_{1x} are considered. T_2 just lets coherences decay
- Relaxation is neglected during the mw and also during rf pulses

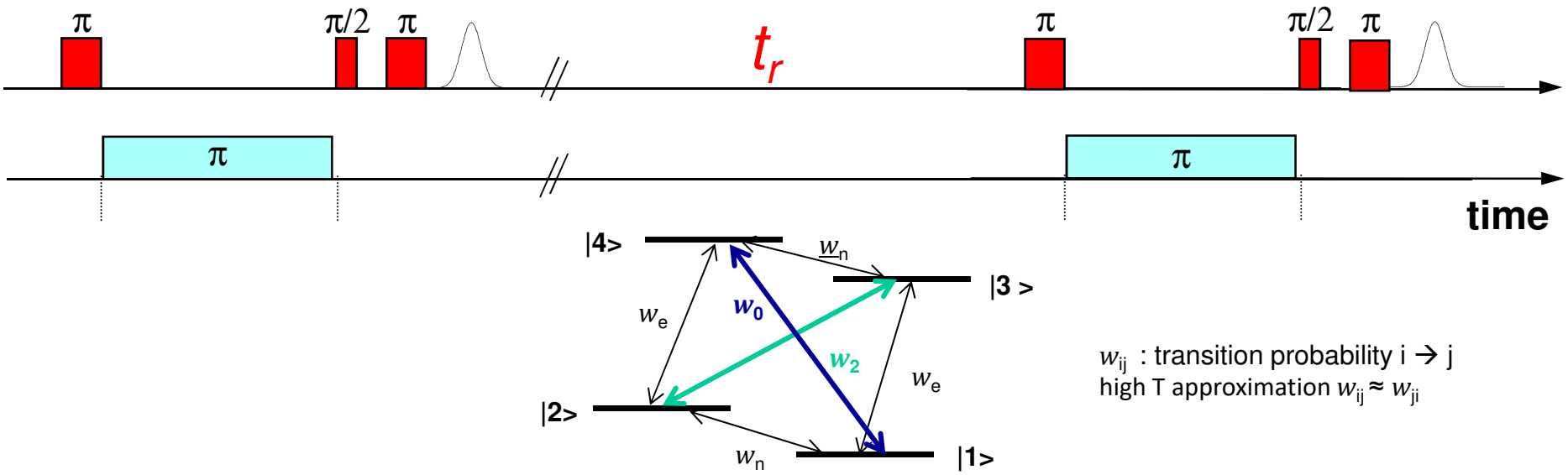

- Take populations N_1, N_2, N_3, N_4 at end of the sequence and let them evolve during repetition time. The result will give the initial population for the next sequence.
- → Solve master equations for N_1, N_2, N_3, N_4

General Solution of Master Equation (Solids)

Two-spin system, high T approximation,

Rizzato & Bennati PCCP 2014

$$\frac{d}{dt}\mathbf{n}(t) = -\mathbf{\Gamma}\mathbf{n}(t)$$ **Master equation**

- Matrix $\mathbf{\Gamma}$ contains the rates w_e, w_n, w_0 , w_2. We set $w_0 \approx w_2 = w_x$ (solid state case)
- Replace population vector **n** = $(N_1, N_2, N_3, N_4)^T$ with new variables containing population *differences* n_{ij} that generate the EPR and ENDOR signals n_S and n_I. 3 independent variables:

$$n_I = (N_1 - N_2) + (N_3 - N_4) = n_{I12} + n_{I34}$$
$$n_S = (N_1 - N_3) + (N_2 - N_4) = n_{S\alpha} + n_{S\beta}$$
$$n_\Delta = (N_1 - N_2) - (N_3 - N_4) = n_{I12} - n_{I34}$$

General solution:

$$\mathbf{n}(t) = e^{-\Gamma t}\mathbf{n}(0)$$

$$\begin{aligned} n_I(t) &= c_1 e^{\lambda_1 t} + c_2 e^{\lambda_2 t} + n_{BI} \\ n_S(t) &= c_3 e^{\lambda_1 t} + c_4 e^{\lambda_2 t} + n_{BS} \\ n_\Delta(t) &= n_{0\Delta} e^{\lambda_3 t} \end{aligned}$$

n_{BS}, n_{BI} Boltzmann population differences of EPR and ENDOR lines

n_Δ Difference in polarization of ENDOR lines

Diagonalization of $\mathbf{\Gamma}$ leads to:

$$\lambda_1 = \frac{1}{T_{1n}} = 2w_n + 2w_x$$

$$\lambda_2 = \frac{1}{T_{1e}} = 2w_e + 2w_x$$

$$\lambda_3 = \frac{1}{T_{1\Delta}} = 2w_e + 2w_n$$

For ENDOR lines $n_{I,12}$ and $n_{I,34}$:

$$\begin{aligned} n_{I,12}(t) &= \frac{1}{4}(2e^{-t\lambda_1}(n_{0,12} + n_{0,34}) + 2e^{-t\lambda_3} n_{0,\Delta}) \\ n_{I,34}(t) &= \frac{1}{4}(2e^{-t\lambda_1}(n_{0,12} + n_{0,34}) - 2e^{-t\lambda_3} n_{0,\Delta}) \end{aligned}$$

Formalism to Include Relaxation in Davies ENDOR

Vega, Goldfarb et al, JMR Vol. 148, p. 388 (2001)

- **Goal: compute intensity of ENDOR line under the effect of relaxation**

- Operators ***P*** represent effect of selective MW or RF π pulses on populations:

$$\begin{pmatrix} n_3 \\ n_2 \\ n_1 \\ n_4 \end{pmatrix}^{+} = P^{13} \begin{pmatrix} n_1 \\ n_2 \\ n_3 \\ n_4 \end{pmatrix}$$

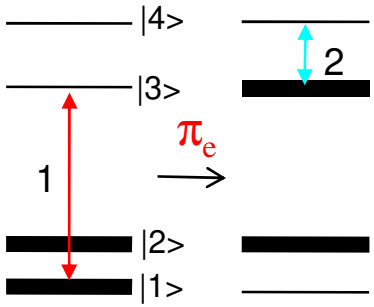

- Relaxation during the mixing time (if t_{mix} long) after first mw π pulse:

$$\mathbf{n}(t_{mix}) = e^{-\Gamma t_{mix}} P^{13} \mathbf{n}(0)$$

- Relaxation during the mixing time after first mw π pulse and rf π pulse :

$$\mathbf{n}(t_{mix}) = e^{-\Gamma t_{mix}} P_{RF}^{34} P^{13} \mathbf{n}(0)$$

- Effect of sequence repetition: after first shot if t_R << T_{1n}, initial state is not n(0): can be solved numerically (must take into account also echo detection)

$$\mathbf{n}(t_R, 1^{rst}\ shot) = e^{-\Gamma t_R} P_{EPR\,\det} P_{RF}^{34} P^{13} \mathbf{n}(0) \qquad \mathbf{n}(t_R, 2^{nd}\ shot) = e^{-\Gamma t_R} P_{EPR\,\det} P_{RF}^{34} P^{13} \mathbf{n}(t_R, 1^{st}\ shot)$$

Relaxation Effects in Variable Mixing Time (VMT) ENDOR

Sign of the hyperfine coupling

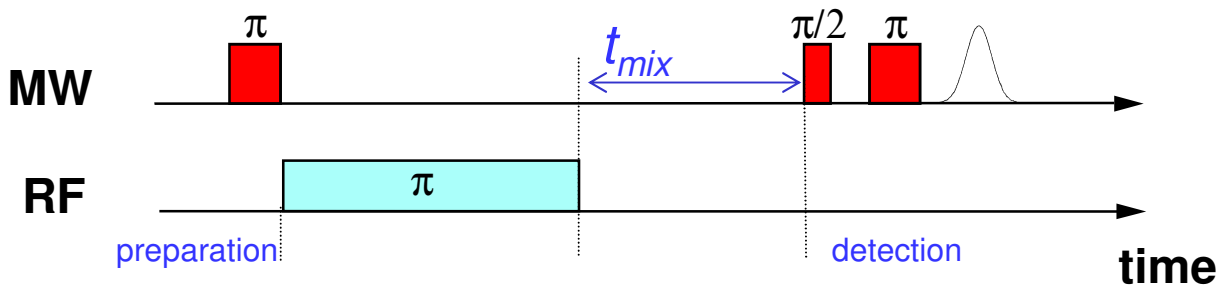

At low T and high EPR frequencies:

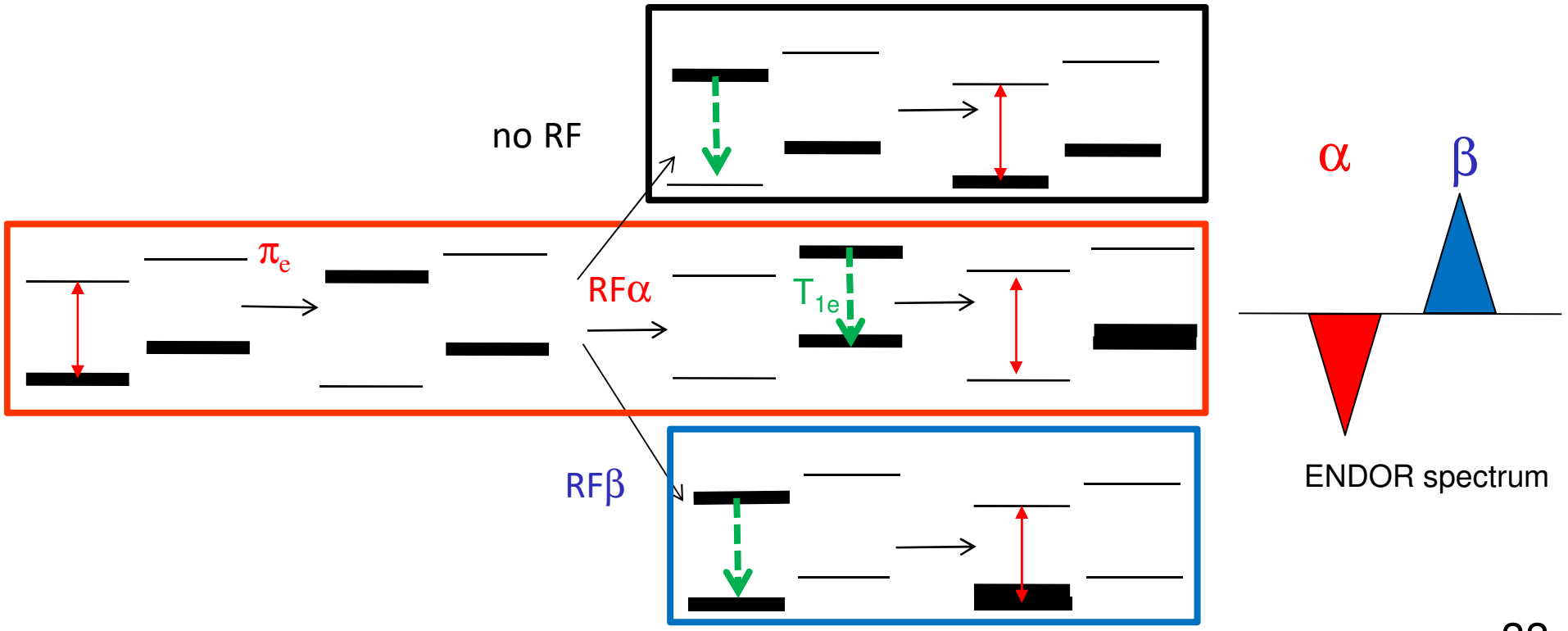

Bennebroek & J. Schmidt, JMR Vol. 128, p. 199 (1997)

VMT ENDOR: Sign of the Hyperfine Coupling

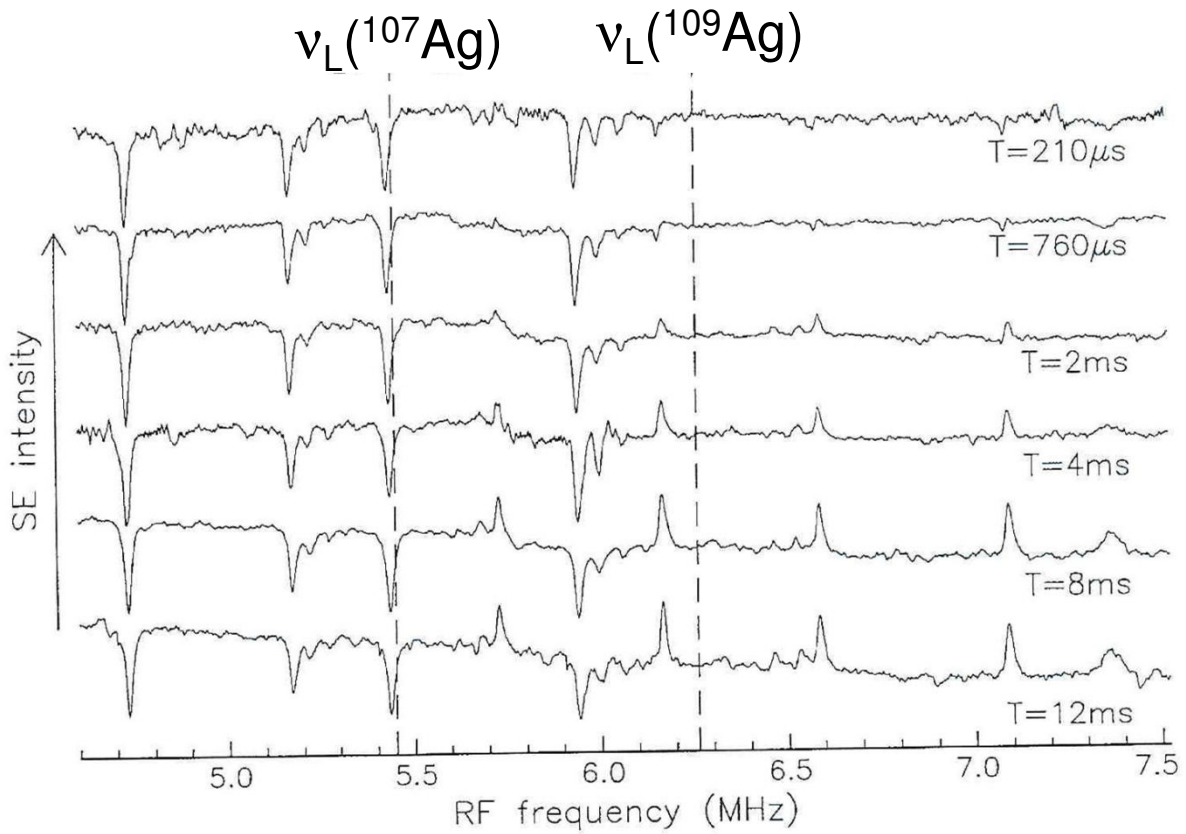

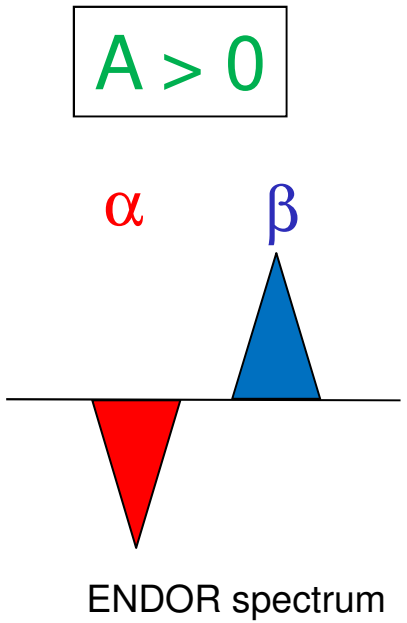

FIG. 6. The effect of spin–lattice relaxation on the intensity of the SE echo in the case of Mims-type ENDOR experiments. The spectra contain ^{107}Ag and ^{109}Ag ENDOR transitions of silver ions surrounding the central $AgCl_6$ unit of the STH complex in AgCl and have been recorded at 1.2 K and at 95 GHz with the magnetic field parallel to the D_{4h} distortion axis of the complex. The interval between the $\pi/2$ MW preparation pulses $\tau = 0.35$ μs and the RF pulse length is taken to be 10 μs shorter than the values of T listed. In addition we have indicated the values of the Zeeman frequencies of ^{107}Ag and ^{109}Ag by $\nu_z(^{107}Ag)$ and $\nu_z(^{109}Ag)$, respectively.

Bennebroek & J. Schmidt, JMR Vol. 128, p. 199 (1997)

Principle of Cross Polarization/CP-ENDOR

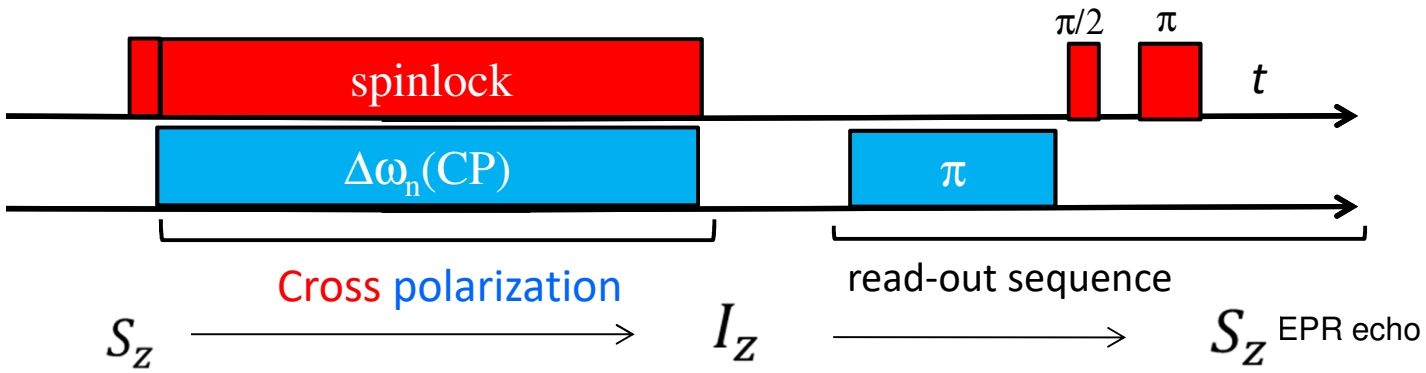

Polarize Nuclei by eNCP

(Electron-Nuclear Cross Polarization)

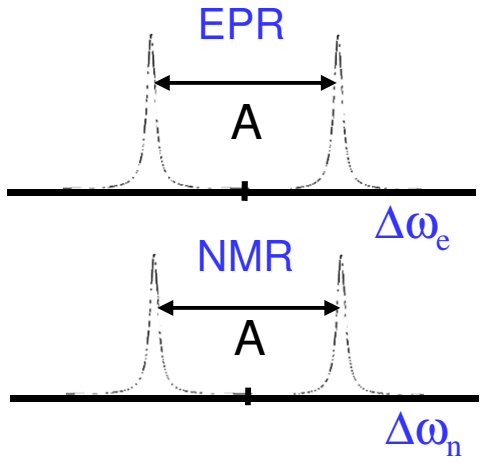

Hamiltonian for S=1/2, I = ½ in doubly rotating frame:

$$\mathcal{H} = \Omega S_z + \omega_{1e} S_x + \omega_{1n} I_x + \Delta\omega_n I_z + A I_z S_z$$

Characteristics of the electron-nuclear case:

$$\omega_{1e} / 2\pi \sim 1 - 10 MHz$$

$$\omega_{1n} / 2\pi \sim 10 - 100 kHz$$

$$A \sim 0 - 100..MHz$$

Weis, Bennati, Rosay Griffin, *JCP 1999*
Weis & Griffin *SSNMR 2006*
Glaser et al. AMR 2008
Rizzato, Kaminker, Vega, Bennati
Molecular Physics 2013

Consequence: NMR Hartmann-Hahn condition cannot be fulfilled:

$$\omega_{1e} \neq \omega_{1n}$$

Description of eNCP

Easiest case: $A << \omega_{1e}$; $\Delta\omega_e = 0$

Rotate Hamiltonian into the direction of the effective microwave field, new Hamiltonian is called ***tilted or dressed state*** Hamiltonian:

$$\mathcal{H}_{tilted} \approx \omega_{1e} S_z^* + \Delta\omega_n I_z + \omega_{1n}\left(I_x^{2-3} - I_x^{1-4}\right)$$

Rizzato, Vega et al, Molecular Physics 2013

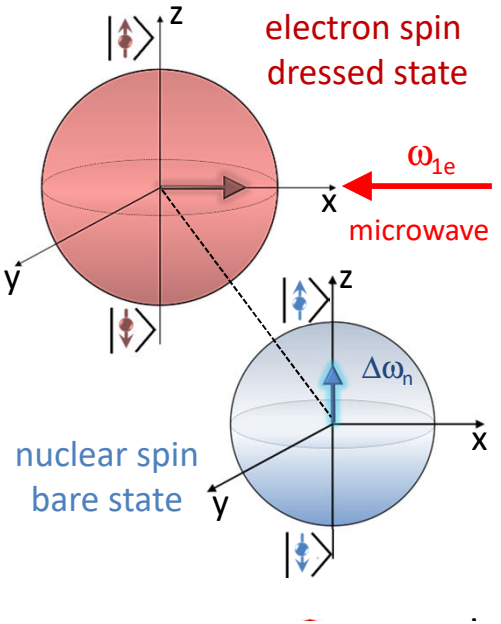

Cross polarization (CP): from ENDOR to DNP

ENDOR

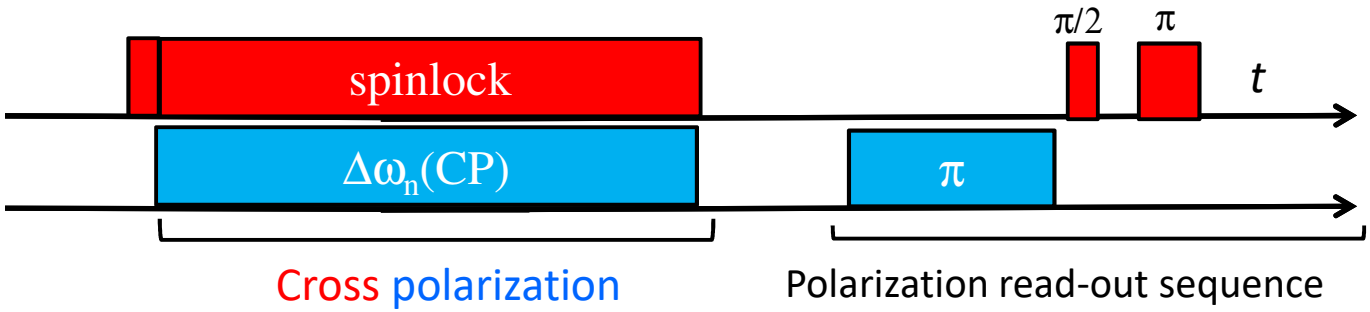

Rizzato et al, Molecular Physics 2013, PCCP 2014

Pulsed DNP

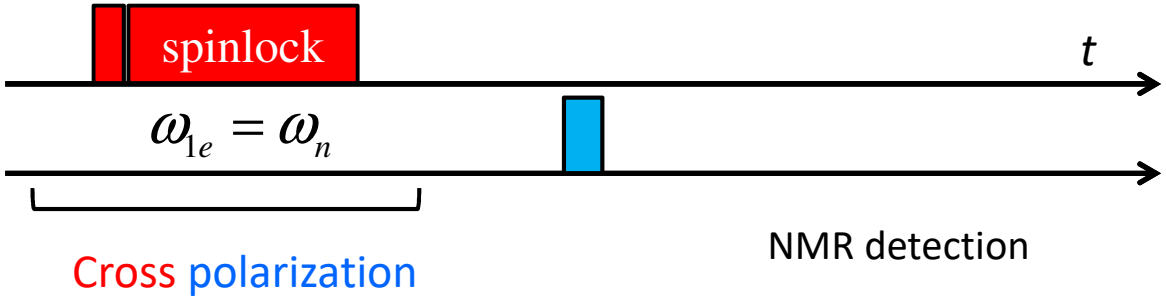

For DNP CP at NOVEL condition has been reported:
Henstra et al. JMR 1988, Can & Griffin et al. JCP 2015, Jain et al. JCP 2017

Bibliography & Further Reading about ENDOR

A. Grupp & M. Mehring, *Pulse ENDOR spectroscopy in solids,* in ‚Modern pulsed and continuous wave electron spin resonance ed. by. L. Kevan and M.K. Bowman, Wiley, New York (1990) p.195

C. Gemperle, A. Schweiger, Pulse electron-nuclear double resonance methodology, *Chem. Rev.* **91**, p. 1481 (1991)

B. Epel , A. Pöppl, P. Manikandan, S. Vega, D. Goldfarb, Effects of spin relaxation in ENDOR spectra recorded at high magnetic fields and low temperatures, *J. Magn. Reson.* **148**, p. 388 (2001)

A. Schweiger and G. Jeschke, *Principles of pulse electron paramagnetic resonance* Oxford University Press, 2001.

M. Bennati, D. Murphy, *EPR spectra in the solid state*, in *EPR: a practitioner's toolkit*, Edited by M. Brustolon and E. Giamello, John Wiley New York (2009)

A.M. Tyryshkin, J. J. L. Morton, A. Ardavan, S. A. Lyon, *J. Chem. Phys.* **124**, 234508 (2006)

R. Rizzato, I. Kaminker, S. Vega, M. Bennati, Cross-polarization edited ENDOR, *Mol. Phys.* **111**, 2809-2823 (2013)

EPR Spectroscopy, Fundamental and Methods, ed. by D. Goldfarb and S. Stoll, John Wiley & Sons (2018)

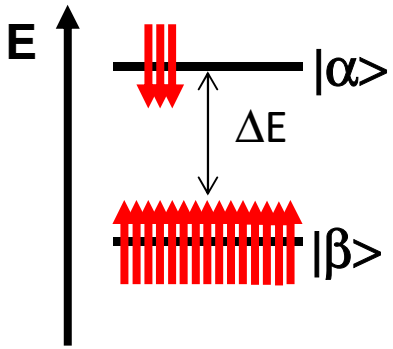

Electron-Nuclear Polarization Transfer

Hyperfine Coupling *A*

e spin

nuclei

ENDOR

A ≥ *10 kHz*

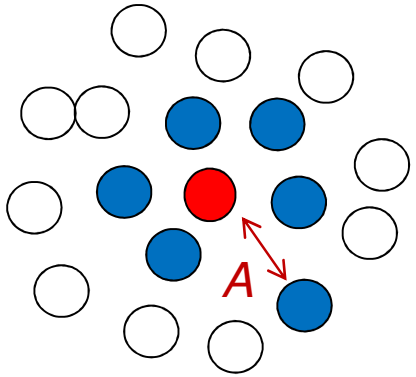

DNP/NMR

A < *10 kHz* (bulk nuclei)

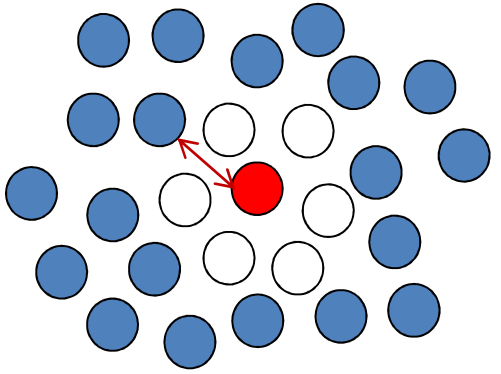

Dynamic Nuclear Polarization

Goal: enhance NMR signals

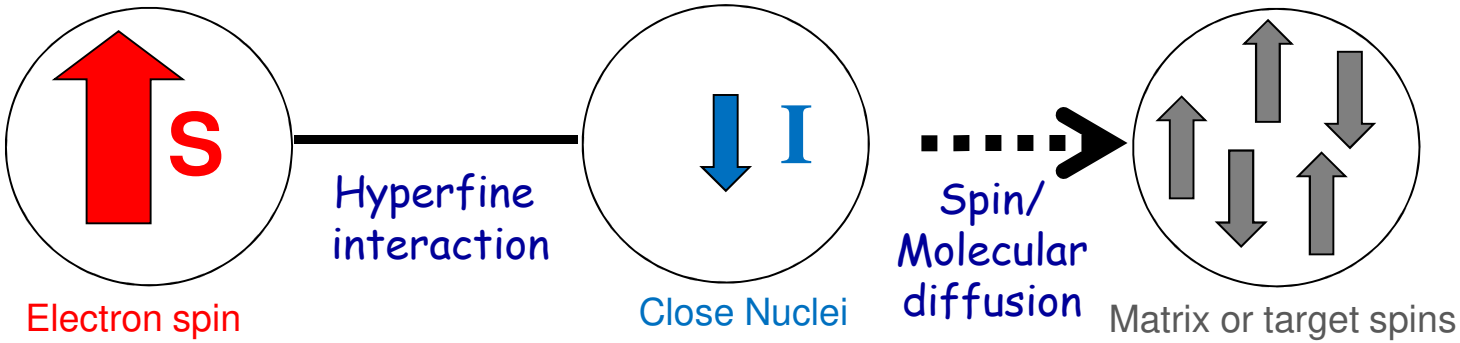

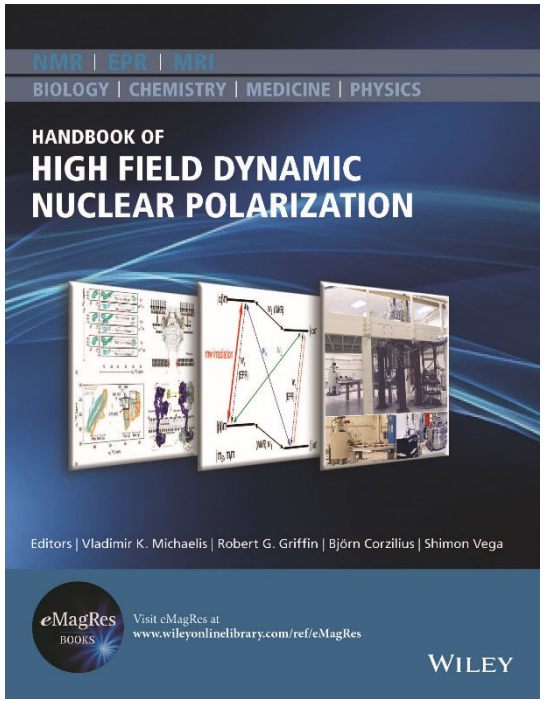

Overhauser DNP
MAS DNP
Dissolution DNP

Spin Polarization

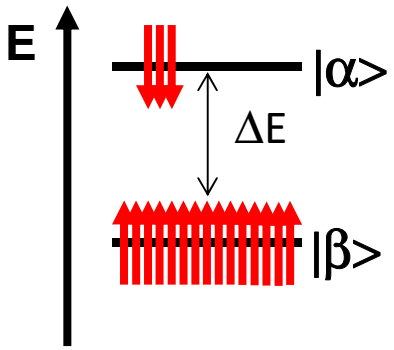

$$P_0 = \frac{N_\alpha - N_\beta}{N_\alpha + N_\beta} = \tanh\left[\Delta E / 2kT\right] \approx \frac{\Delta E}{2kT}$$

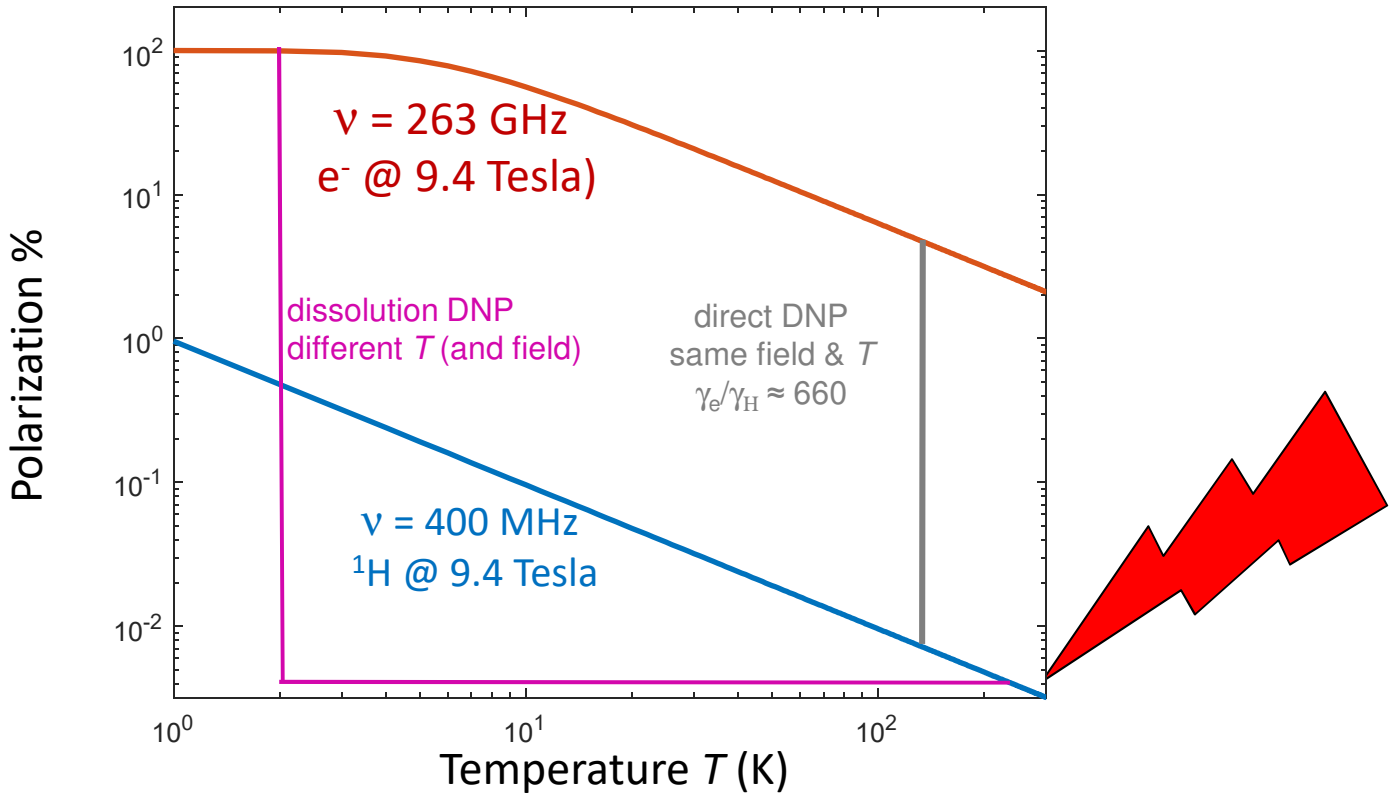

Overhauser DNP in Metals and Liquids

first discovered mechanism in 1953

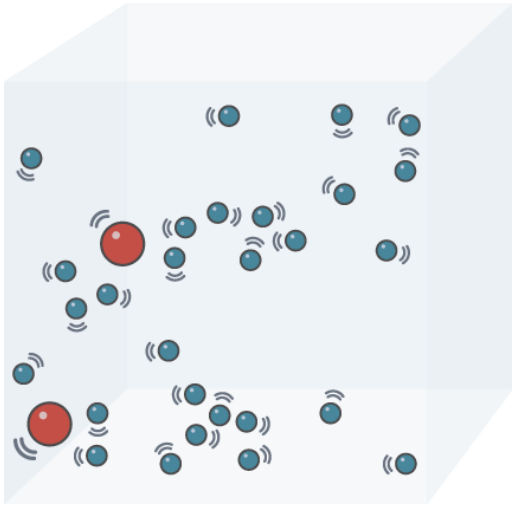

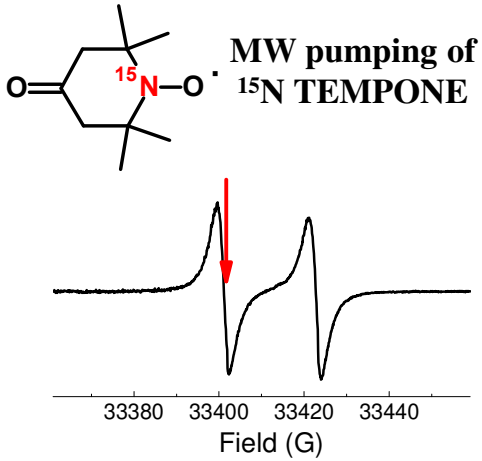

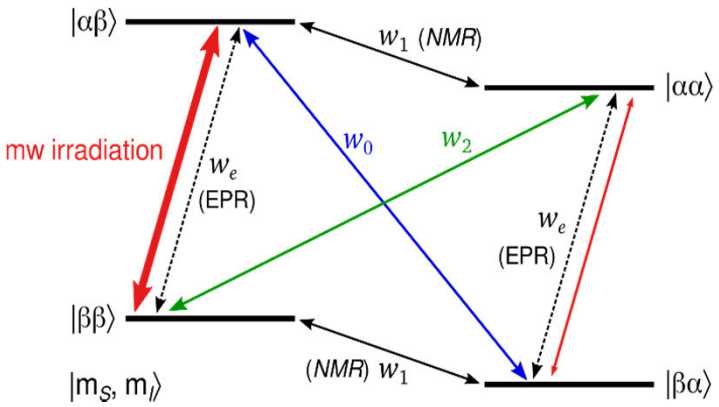

……. driven by relaxation due to motion that modulates hf interaction

$$\varepsilon = \frac{\langle I_z \rangle}{\langle I_0 \rangle} = 1 - \xi \cdot f \cdot s_{eff} \cdot \frac{|\gamma_e|}{\gamma_I}$$

Hausser & Stehlik 1968

DNP Induced by Scalar and Dipolar Relaxation

$$\xi = \frac{w_2^{dip} - w_0^{dip} - w_0^{scalar}}{w_0^{dip} + 2w_1^{dip} + w_2^{dip} + w_0^{scalar}}$$

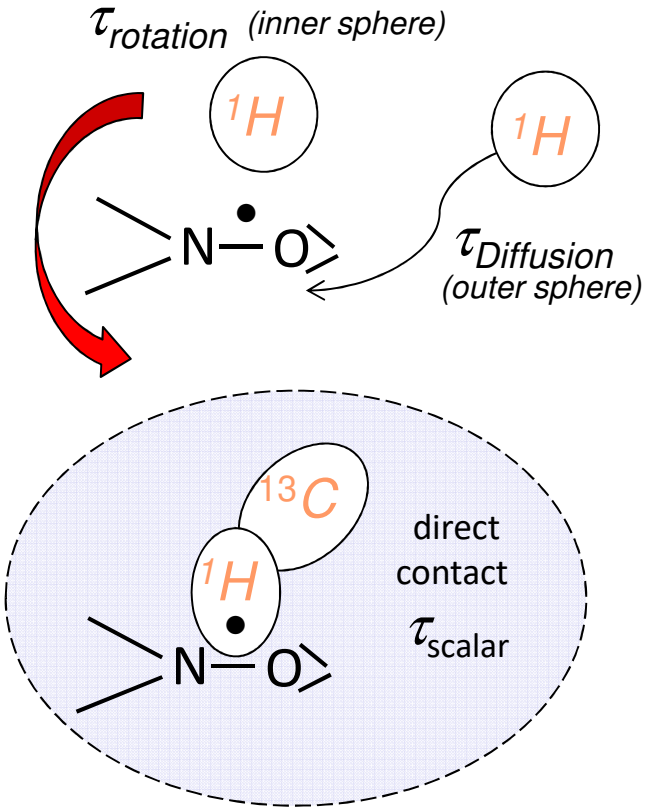

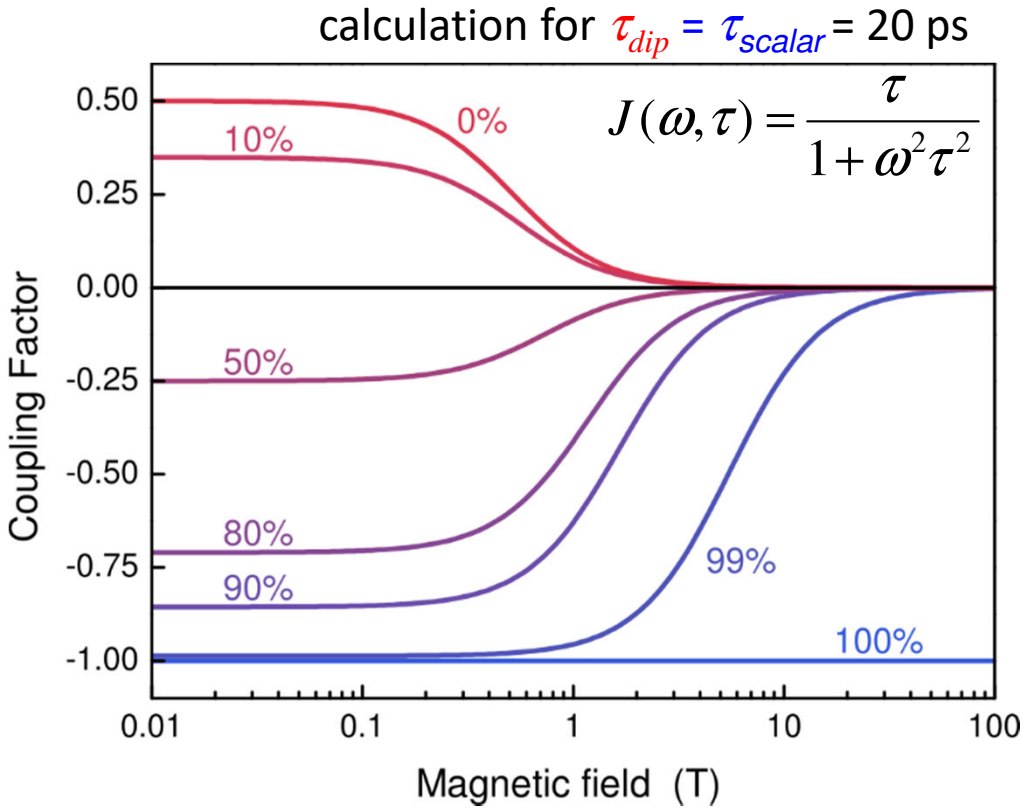

M. Bennati & T. Orlando
Handbook of HF-DNP, Chapter 14

Water Coupling Factors for Hydration Dynamics

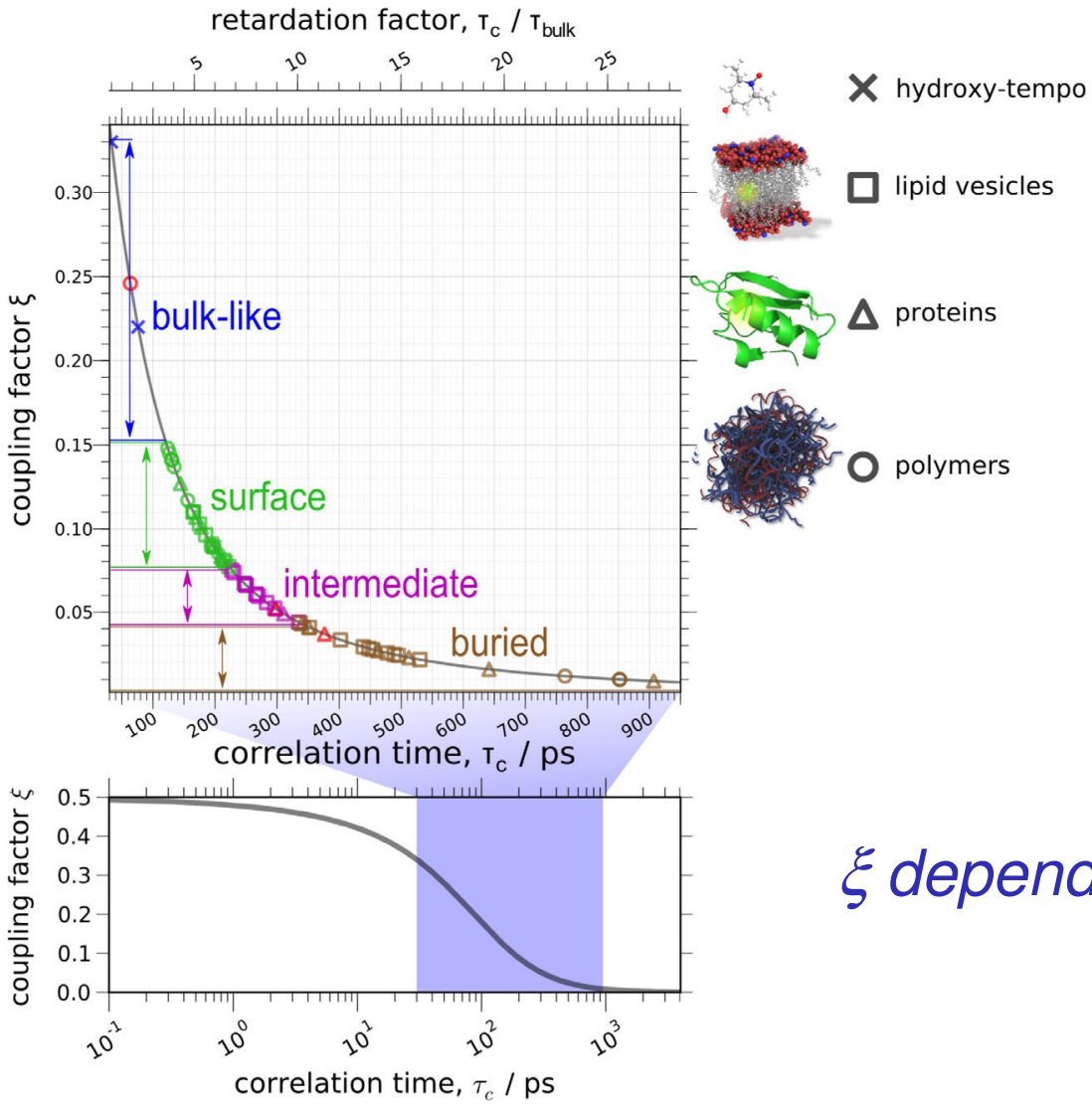

ξ depends on τ

J. Franck, A. Pavlova, J. Scott, S. Han, Prog. NMR Spectr. 2013

260 GHz/ 9 T ^{1}H DNP on Aligned Lipid Bilayers

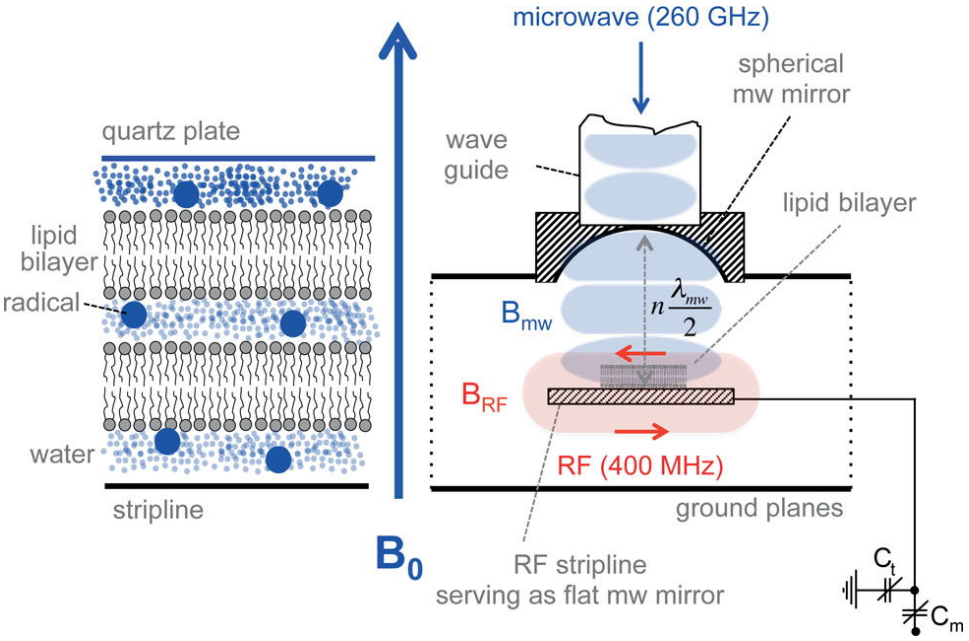

A thin stack of lipid bilayers is placed on a metal stripline, which creates the B1-RF field at the surface and produces the FID. The stripline together with an opposite spherical mirror forms a microwave resonator.

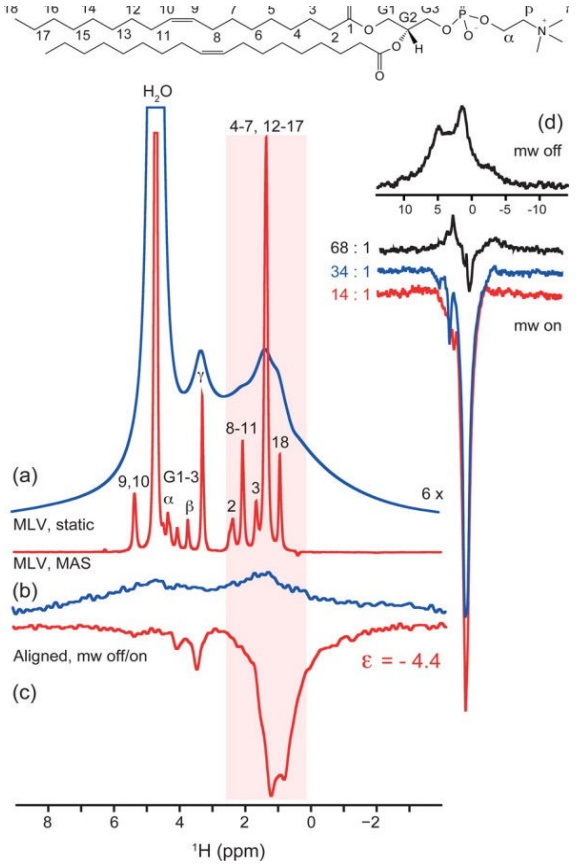

(a) 1H NMR spectra of DOPC vesicles (static and MAS at 600 MHz). (b) 1H NMR spectrum of DOPC aligned as shown in Figure 1, doped with TEMPOL (DOPC:TEMPOL 34:1), and hydrated with D2O (DOPC:D2O 1:27), resulting in a stack of approximately 2000 bilayers of 20 μm thickness. (c) Upon microwave irradiation (5.6 W), an enhancement of −4.4 was observed for the acyl chain proton resonances. (d) The enhancement increases with the amount of TEMPOL present.

O. Jakdetchai; V. Denysenkov; J. Becker-Baldus; B. Dutagaci; T. F. Prisner; C. Glaubitz; J. Am. Chem. Soc. ***2014,*** *136, 15533-15536.*

High-resolution ^{13}C-DNP/NMR at 9.4 T/400 MHz

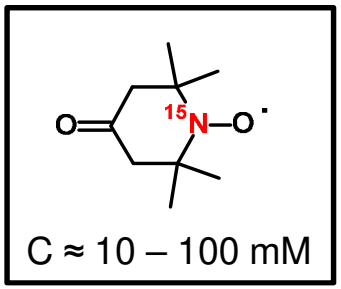

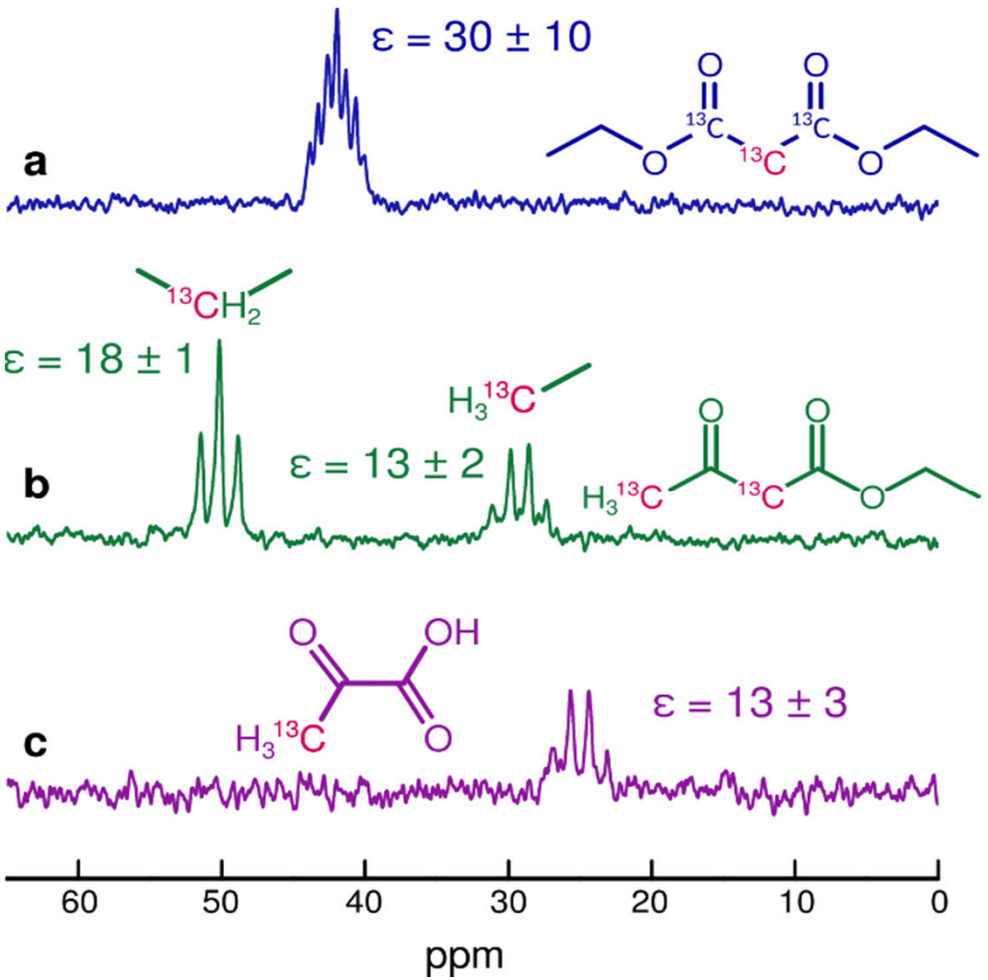

➢ *About a factor of 900 shorter acquisition time !*

T. Orlando, R. Dervisoglu, M. Levien, I. Tkach, T. Prisner, L. Andreas, V. Denisenkov & M. Bennati, Angewandte Chemie 2019, 58, 1402-1406

MAS Solid State DNP

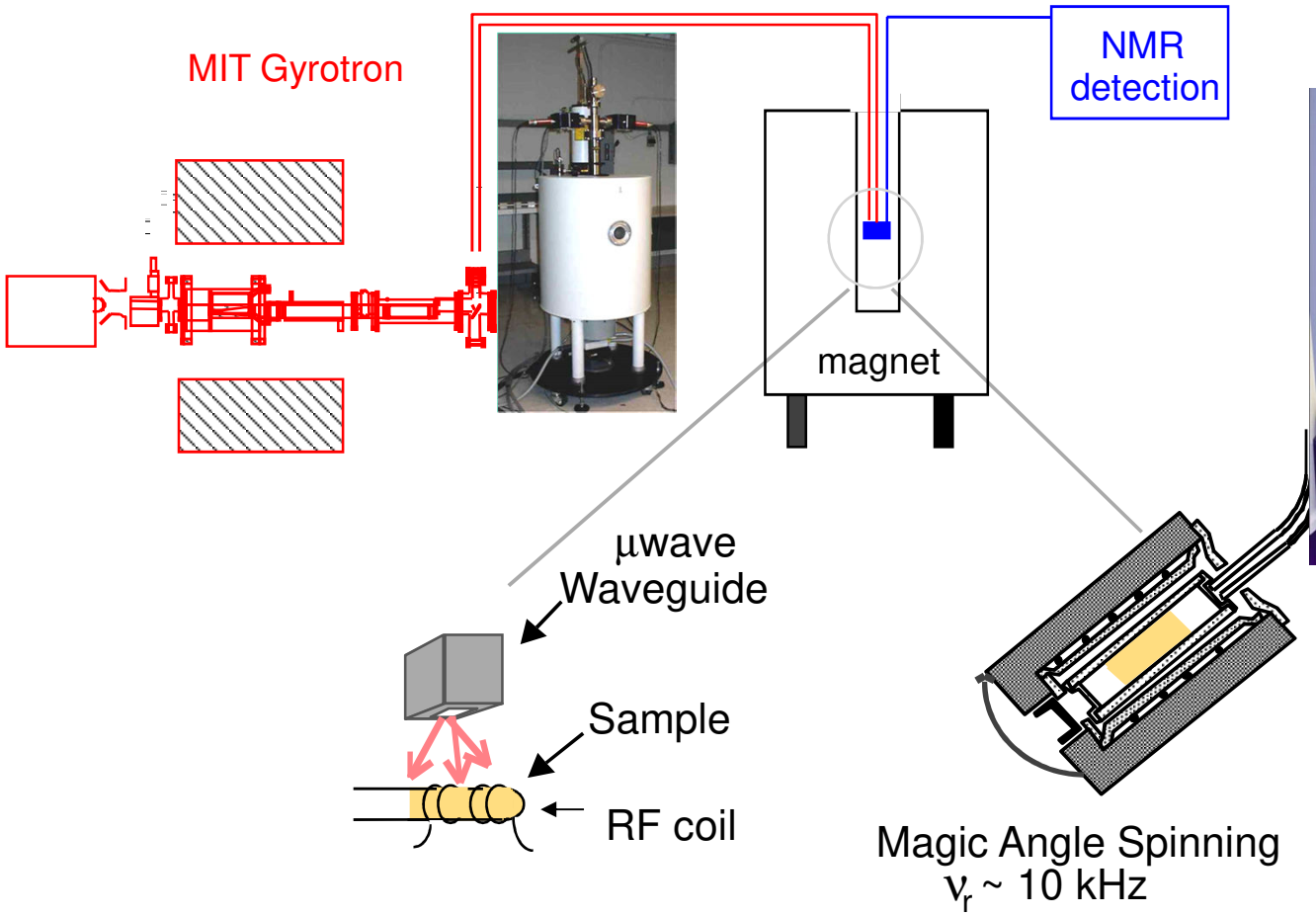

Bruker 263 GHz gyrotron

Rosay et al., PCCP 2010

Hall , Griffin et al., Science, 1995

Cross Effect/Thermal Mixing

interacting paramagnetic centers

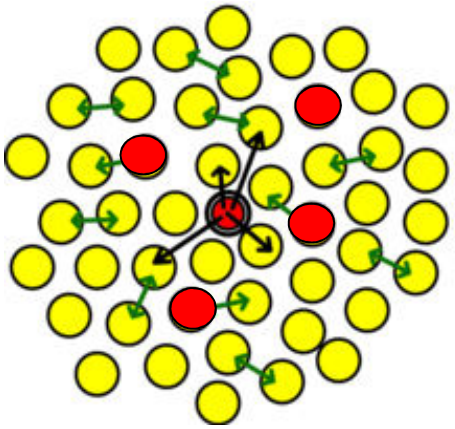

TM case

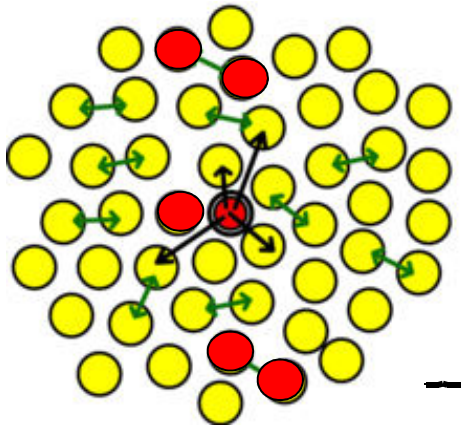

CE case

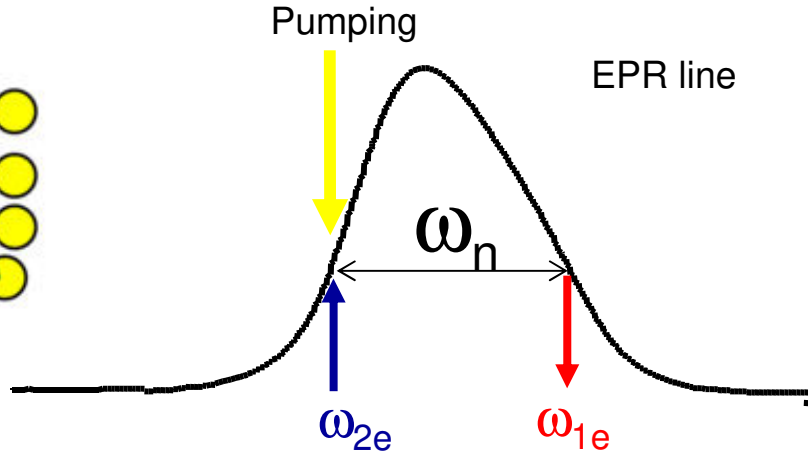

Energy conserving three particle mechanism:

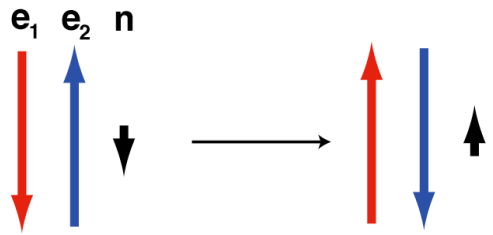

$\omega_{2e} - \omega_{1e} = \omega_n$

C.F. Hwang and D.A. Hill, PRL *18,* 110-112 (1967)

Wind et al., Adv. Opt. Magn. Res. (1985)

probability $\propto \omega_n^{-1}$

Recent review:
S. Vega et al., Handbook of DNP, Chapter 2

Tailored bi-radicals for cross-effect:
EPR resonance differs exactly by ω_n

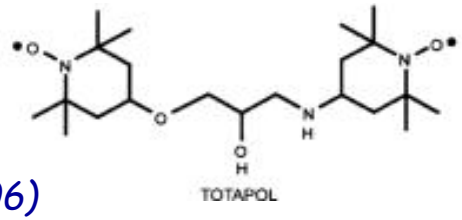

(Griffin et al. 2006)

Dynamic Nuclear Polarization of Cellular Lysates

K. Frederick et al, Cell Vol. 163, p. 620-628

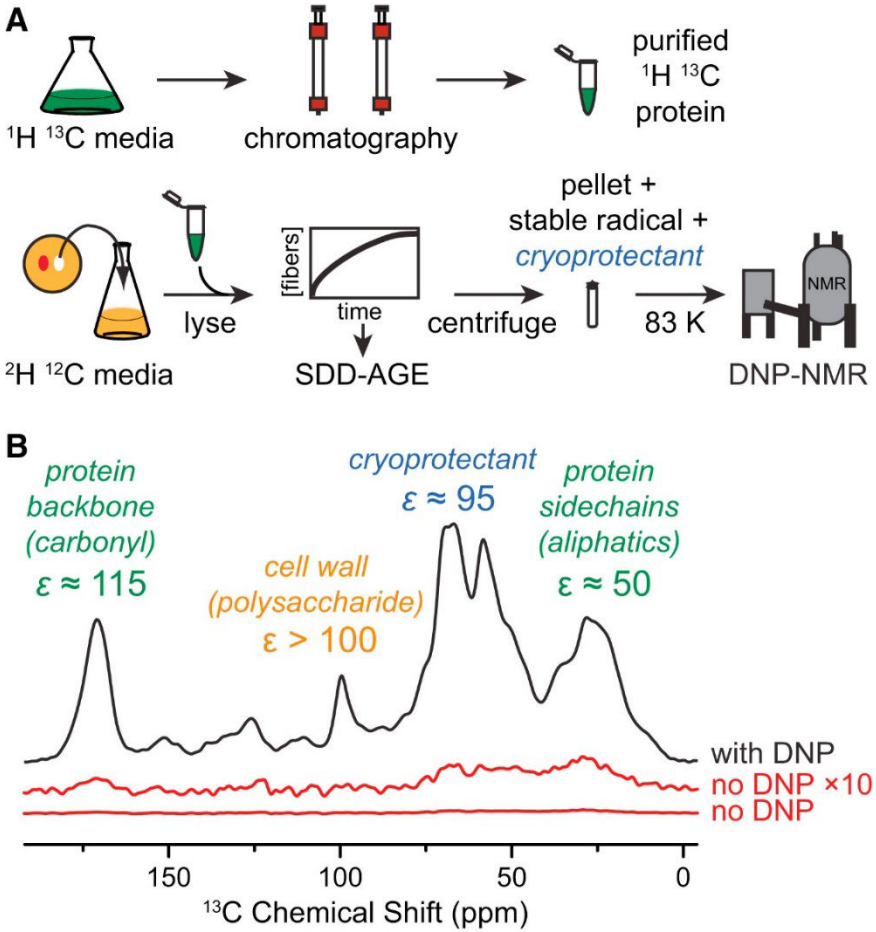

(A) Preparation of samples for DNP MAS NMR of proteins at endogenous levels in biological environments. The protein of interest is expressed on isotopically enriched media and purified. The cellular background comes from cells grown on media containing D_2O. The cells are lysed and the isotopically labeled protein is added exogenously to whole lysate. The mixture is pelleted, the pellet is resuspended in a matrix containing stable radical and cryoprotectant, and the mixture is frozen for analysis by DNP MAS NMR.

(B) One-dimensional ^{13}C spectra both with (black) and without DNP enhancement by microwaves (red). Dynamic nuclear polarization gave large signal enhancements (ε) for uniformly ^{13}C-labeled of the prion region of Sup35 protein (amyloid fibrils) in a deuterated matrix of cellular lysates containing a 60:30:10 (v/v) mixture of *d8*-glycerol:D_2O:H_2O and 10 mM TOTAPOL at 211 MHz/140 GHz with $\omega/2\pi$ = 4.3 kHz and a sample temperature of 83 K.

DNP Surface Enhanced (DENS) NMR Spectroscopy

C. Coperet et al, Curr. Opin. Coll. Inter. Sci. 2018, p. 63

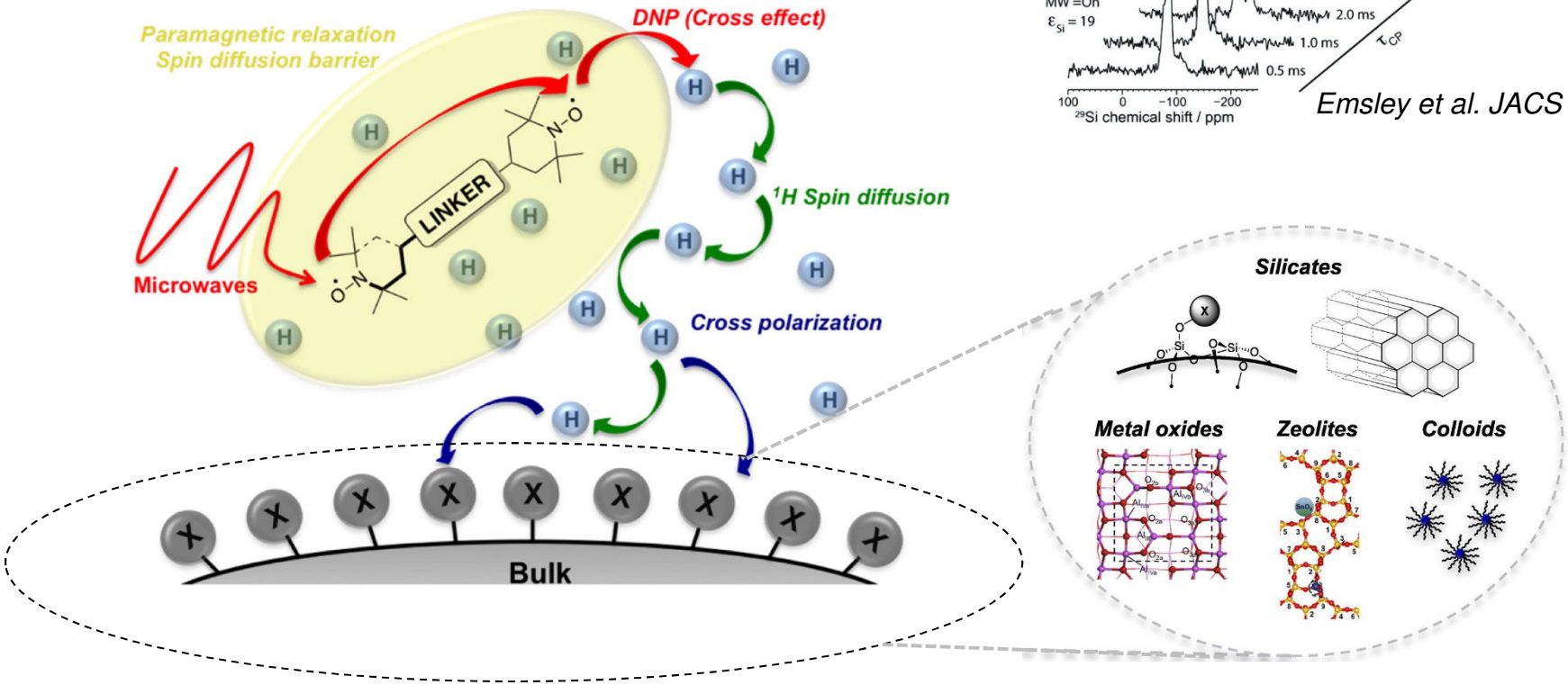

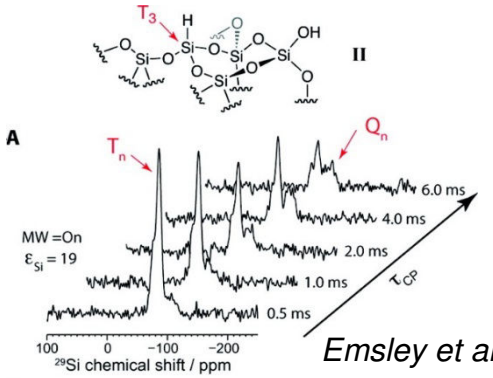

Emsley et al. JACS 2011

See also, A. Lesage et al, Handbook of HF-DNP 2019, Chapter 18

Dissolution DNP

Polarize the sample at 1.5 K and transfer rapidly into another magnet

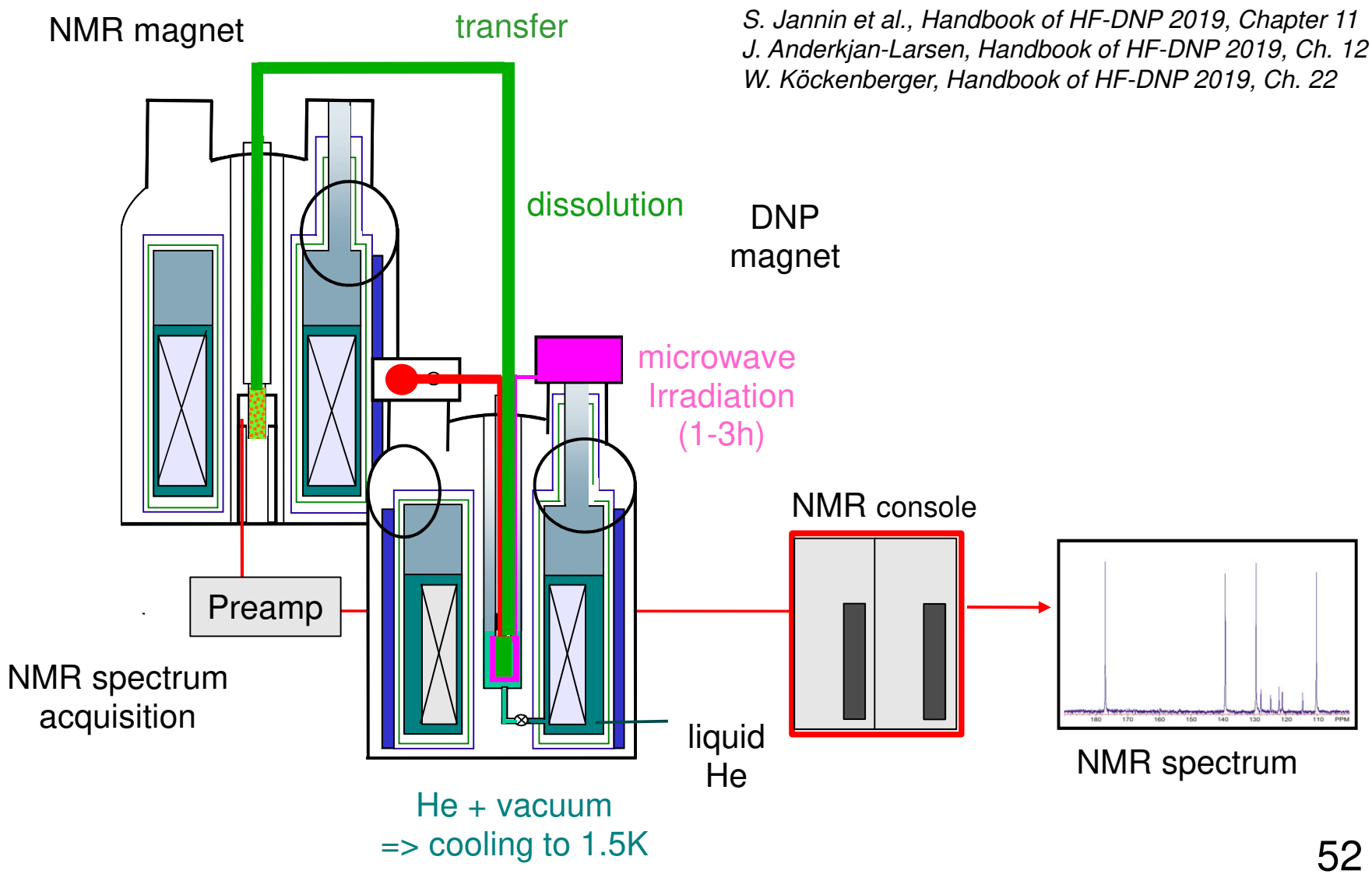

S. Jannin et al., Handbook of HF-DNP 2019, Chapter 11
J. Anderkjan-Larsen, Handbook of HF-DNP 2019, Ch. 12
W. Köckenberger, Handbook of HF-DNP 2019, Ch. 22

Solid Effect

Isolated paramagnetic centers

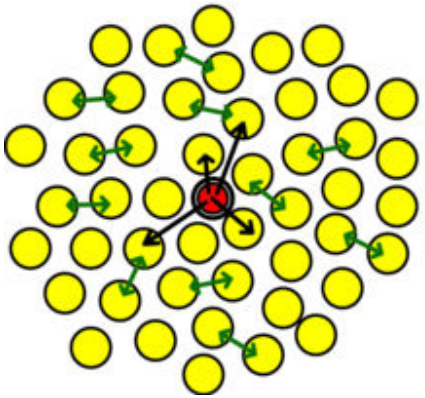

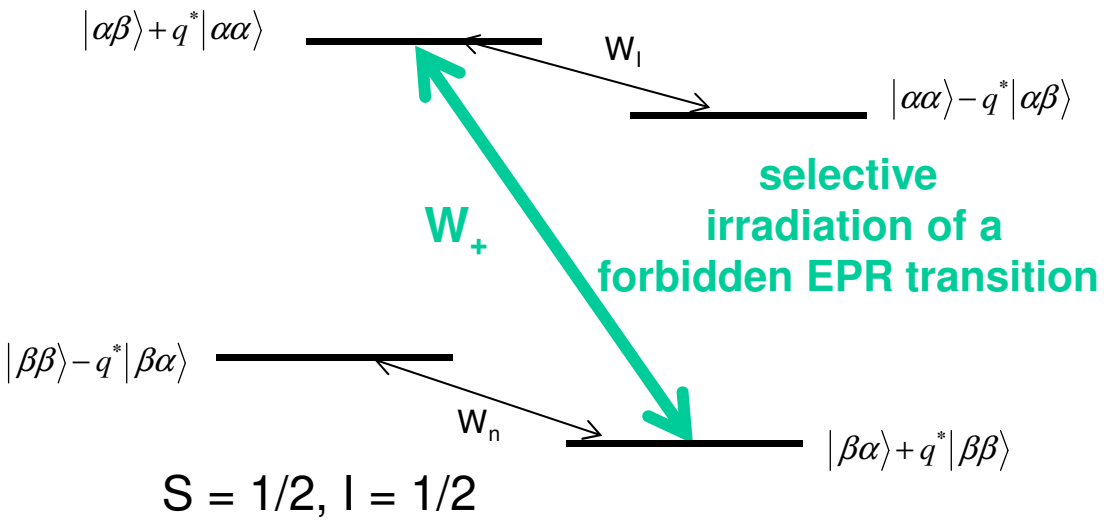

Mixing coefficients
from anisotropic hfc:

$$q_{ij} = -\frac{3}{4}\frac{\gamma_e\gamma_n\hbar}{\omega_n}\frac{1}{r_{ij}^3}\sin\theta_{ij}\cos\theta_{ij}e^{-i\phi_{ij}}$$

$$W^{\pm} = 2\left|q_{ij}\right|^2 \pi\gamma_e^2 B_1^2 g(\omega_e - \omega \pm \omega_n)$$

$$\varepsilon = \frac{\langle I_z \rangle}{I_0} = 1 + \frac{W^+}{W^+ + W_n}\left(\frac{|\gamma_e|}{\gamma_n} - 1\right) \approx \frac{|\gamma_e|}{\gamma_n}$$

R. Wind et al. 1985

Recent theoretical treatment for multispin system including relaxation:
S. Vega et al., JCP 2011

Application Areas of Dissolution DNP

^{13}C-pyruvate, MRI

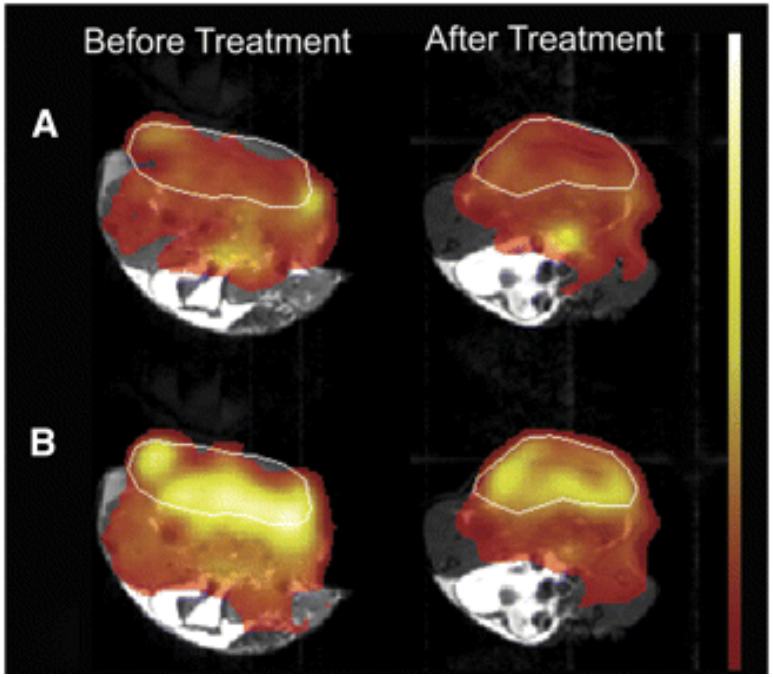

In vivo tumor biochemistry with ^{13}C-DNP MRI
Gallagher et al. J. Nucl. Med. 2011

Enzymology

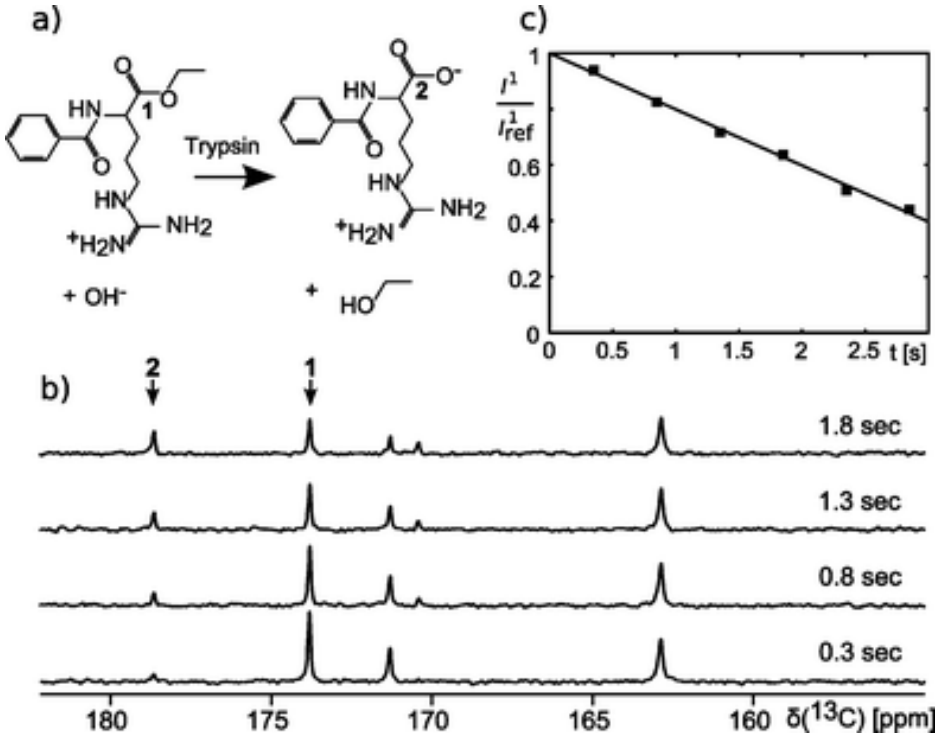

Time-resolved ^{13}C DNP-NMR follows enzymatic reactions
Hilty et al. Org. Biomol. Chem. 2011